Hydrologic history and flooding pulses control iron and sulfur metabolic composition with variable associations to greenhouse gas production in a coastal wetland mesocosm experiment

Colin G. Finlay[a]#, Ariane L. Peralta,[a]

[a] Department of Biology, East Carolina University, Greenville, North Carolina, USA

Running Head: Microbial response to hydrology and flooding pulses

#Address correspondence to Colin G. Finlay, finlayc21@students.ecu.edu.

Abstract and Importance word count: 366

Text word count (excluding methods, references, tables, figure legends, and supplemental material): 5,114

Open Research statement: All code and data used in this study are in a public GitHub repository (https://github.com/PeraltaLab/WetlandMesocosm_GHG_Timberlake) with a Zenodo DOI (10.5281/zenodo.4042109, to be updated). Raw amplicon sequence files can be found at NCBI SRA BioProject ID PRJNA636184, and metagenome sequence files can be found at NCBI SRA BioProject ID PRJNA641216.

Key words/phrases: iron, sulfur, saltwater intrusion, flooding, plant cover

ABSTRACT

Coastal wetlands can store carbon by sequestering more carbon through primary production than they release though biogenic greenhouse gas production. The joint effects of saltwater intrusion and sea level rise (SWISLR) and changing precipitation patterns alter sulfate and oxygen availability, challenging estimates of biogenic greenhouse gas emissions. Iron-rich soils have been shown to buffer soil sulfidization by sequestering sulfide into iron-sulfide. But as SWISLR increases soil sulfate concentrations, sulfide produced via sulfate reduction will likely exceed the buffering capacity of soil iron, allowing toxic sulfide levels to accumulate. We used a soil mesocosm approach to examine the influence of hydrology (wet, dry, interim) and plant presence (with or without plants) on wetland soils sourced from different hydrologic histories at a restored coastal wetland. We hypothesized that reducing conditions (i.e., flooded, no plants) impact anaerobic metabolisms similarly, whereas oxidizing conditions (i.e., dry, plant presence) disrupt coupled sulfate reduction and iron reduction. Over eight weeks of hydrologic manipulation, 16S rRNA amplicon sequencing and shotgun metagenomic sequencing were used to characterize microbial communities, while greenhouse gas fluxes, soil redox potential, and physicochemical properties were measured. Results showed that contemporary hydrologic treatment affected assimilatory sulfate reduction gene composition, and hydrologic history influenced dissimilatory sulfate reduction and iron reduction gene composition. Sulfate and iron reduction genes were correlated, and dissimilatory sulfate reduction genes explained variance in methane fluxes. These findings highlight the role of historical hydrology, potential saltwater exposure, and soil iron in shaping microbial responses to future changes in soil moisture and salinity.

IMPORTANCE

Understanding the microbial community metabolism of coastal wetland soils is crucial for predicting their role in carbon sequestration and greenhouse gas emissions under future climate scenarios. This study highlights how historical hydrology and past saltwater exposure influence microbial processes in wetland soils, particularly sulfate and iron reduction and their interactions with greenhouse gas production. By elucidating the interactions between hydrology, plant presence, and microbial communities, our findings provide valuable insights into the resilience and vulnerability of coastal wetlands to pulses of flood, drought, and vegetation clearance. This knowledge is essential for predicting climate change impacts on wetland carbon budgets, developing effective management strategies to mitigate climate change impacts, and preserving the ecological functions of these vital ecosystems.

INTRODUCTION

Coastal freshwater wetlands are major sinks for atmospheric carbon (C) and reactive nitrogen (N) (1–3). But these ecosystem services are threatened by saltwater intrusion and sea level rise (SWISLR) (4–7), changing precipitation patterns (8–10), and loss of wetland vegetation (1, 3). SWISLR can impose flooded conditions and the influx of terminal electron acceptors (TEAs) such as sulfate (SO_4^{2-}) (11, 12). Flooding alters the TEA pool, by decreasing soil oxygen (O_2) levels (13), and saltwater intrusion from marine sources introduces SO_4^{2-} to the ecosystem (11, 14, 15). The combined impacts of flooding and SO_4^{2-} addition on wetland ecosystem function are difficult to predict, in part because varying environmental characteristics, especially soil ferrous iron (Fe(II)), could buffer the effects of SO_4^{2-} intrusion (15–17). With climate change predicted to increase rates of sea level rise and increase frequency of storm surges from more intense tropical storms, we need to better understand how the combined environmental stressors, saltwater intrusion and flooding, influence coastal wetlands (18).

To harvest energy through respiration, microorganisms oxidize organic or inorganic substances, and transfer the electrons through electron transport chains, to ultimately reduce a TEA (19). O_2 is used as a TEA in aerobic respiration (reviewed in Glass et al., 2022); in the absence of O_2, a variety of other TEAs may be used in anaerobic respiration, including nitrate (NO_3^-), ferric iron (Fe(III)), SO_4^{2-}, and carbon dioxide (CO_2) (21) (Figure 1). In common with these respiratory (i.e., dissimilatory) processes, assimilatory processes also involve oxidation-reduction (redox) reactions (19). The availability of specific reductants (e.g., organic matter), and specific oxidants (e.g., TEAs like O_2) modulate both dissimilatory and assimilatory processes (19). The soil redox potential, which is the overall propensity of a soil environment to reduce or oxidize, integrates

relative levels of reductants and oxidants within the soil (19). In this study, we also refer to the overall oxidation-reduction propensity of the environment as "redox status".

Soil redox potential influences microbial community structure and function (22, 23). As soil microbes are major drivers of biogeochemical cycles, soil redox potential affects microbial metabolic capacity, ultimately influencing transformations of C, N, sulfur (S), and Fe at the ecosystem level (21, 24–26). While the prediction of microbial metabolic diversity is inferred by taxonomic approaches, characterizing microbial metabolic diversity by examining genetic potential (e.g., shotgun metagenomics) provides a more direct evaluation of functional potential (27, 28). To further improve prediction of microbial functions, it is critical to understand how changing environmental conditions directly affect soil redox conditions.

Dynamic wetland hydrology modifies soil redox status (23). Flooding of soils fills pore space, thereby restricting access to atmospheric O_2 (29). This creates suboxic and anoxic conditions, requiring alternative TEAs to be used in anaerobic respiration (30, 31) (Figure 1). Based on the hydrologic regime of a wetland, soils therein may experience fluctuating wet-dry conditions, as well as prolonged inundation or dry down (22, 23, 31).

In addition to dynamic hydrology, human activities modify biogeochemical cycles. For example, watersheds accumulate N via human activities, and this N may be loaded in coastal wetlands via hydrologic flows and atmospheric deposition (32, 33). The incoming anthropogenic N may be in the form of NO_3^- or converted to NO_3^- by internal microbial processing (e.g., nitrification, $NH_4^+ \rightarrow NO_3^-$) (34). Since NO_3^- is an efficient TEA, it is used in facultative anaerobic respiration, which is a common metabolism observed in fluctuating oxic/anoxic conditions (35). In addition, saltwater intrusion events can increase soil and porewater SO_4^{2-} concentrations (36). Then, SO_4^{2-}-reducing microorganisms (SRM) produce sulfide which binds with reduced Fe to form

iron sulfide (FeS) (15). This buffering of seawater SO_4^{2-} is, therefore, dependent on the activity of SRM and Fe-reducing microorganisms (FeRM), as well as the existing soil Fe concentrations (15).

While human activities influence biogeochemical cycles, cross-kingdom interactions between plants and microorganisms also have important consequences for soil redox activity. Plants alter soil redox potential by delivering O_2 to the rhizosphere, and transporting CO_2 and methane (CH_4) from the rhizosphere to the atmosphere (37). Plant root O_2 release can buffer the effects of flooding on soil aeration (13, 38, 39). While hydrologic status can be variable over time, plants impose a more constant influence on soil redox conditions (39).

The biogeochemical cycles of C, N, Fe, and S are not isolated, but instead, closely linked. For example, NO_3^- reduction can be coupled to sulfide oxidation (40). The oxidation of organic C is coupled to reductions of NO_3^-, Fe(III), and SO_4^{2-} (19). The microbial N cycle forms an interconnected network, with many reactions dependent on availability of C, Fe, and S (34). Therefore, to understand the cycling of any one element, it is essential to consider the relevant microbe-microbe and microbe-environment interactions that influence the nutrient cycling network.

These microbial nutrient cycling networks provide crucial context for understanding specific environmental phenomena, such as SWISLR and Fe buffering of ecosystem sulfidization. Past work on saltwater intrusion and Fe-S buffering was conducted at the Timberlake Observatory for Wetland Restoration (TOWeR) (15). The TOWeR site is prone to seasonal, drought-induced saltwater intrusion, which introduces SO_4^{2-} to Fe-rich soils (14, 15, 41). Both the SO_4^{2-} and Fe can be microbially reduced to sulfide and ferrous iron (Fe(II)), respectively (15, 41, 42). The sulfide may be toxic to salinity-naïve ecosystems, but can readily bind Fe(II) to create FeS, which is non-toxic and relatively non-bioavailable (15, 41). For example, Schoepfer and colleagues (2014)

found that the pool of reduced Fe in TOWeR soils is sufficient to sequester sulfide from seasonal saltwater intrusion into FeS, but as SWISLR accelerates soil sulfidization, toxic sulfide levels may accumulate in the future.

How future sulfidization (due to SWISLR) will modify wetland microbial community structure and function is unknown. Specifically, it is unclear how wetland microbes that participate in S cycling will respond to flooding/drought, and changes in plant cover. This study used a manipulative mesocosm approach to address the questions (1) how do soil Fe and S concentrations interact with altered redox states (hydrology and plants) and microbial community composition of SO_4^{2-} reduction genes? and (2) how do these Fe-S metabolic associations relate to greenhouse gas (GHG) emissions, mediated by C and N metabolisms? We hypothesize that the most reducing conditions (i.e., prolonged flooding, no plants) modify different anaerobic metabolisms in similar ways and predict that (i) in oxidizing conditions (dry and/or plant presence) the composition of microbes that could participate in SO_4^{2-} reduction and Fe reduction will not be linked/coupled. Coupled here means a significant correlation (i.e., Mantel test) between Bray-Curtis distance matrices of SO_4^{2-} reduction and Fe reduction. We also predict that (ii) in reducing conditions (wet and/or plant absence) coupling between the composition of microbes that could participation in SO_4^{2-} reduction and Fe reduction will be observed, and these processes will contribute to CO_2 production (fit with CO_2 fluxes using envfit) while competing with methanogenesis (observed as negative relationship with methanogenic functional genes and CH_4 fluxes).

METHODS

Sampling and Mesocosm Experimental Design

On April 1, 2016, soil samples were collected from TOWeR located in the Albemarle Peninsula in Tyrell County, North Carolina, USA (35°54’22” N, 76°09’25” W) (43, 44). The site is connected to the Albemarle Sound via the Little Alligator River, with potential for saltwater intrusion (14). Across the sampling area, the position of the water table creates a hydrologic gradient, with sites categorized as dry (upland), wet (saturated), and interim (transition dry/wet) (12) (Figure 2).

Soil blocks collected from the three sites within TOWeR (dry, wet, interim) were used to set up a mesocosm experiment. Soil history was categorized according to water table levels at the time of collection (dry = 20 cm, interim = 10 cm, and wet = 0 cm below surface level). Six intact soil blocks (25 cm x 25 cm x 20 cm) from each of the three hydrologic histories were contained in dark plastic containers of the same dimensions. Soil mesocosms were maintained for the duration of the experiment at the East Carolina University (ECU) West Research Campus (Greenville, NC) under a covered hoop house with a shade cloth to prevent precipitation while allowing 60% light penetration. Each block was divided in half by a root screen (20 µm stainless steel mesh). Plants were allowed to grow on one side of the screen and removed (above- and belowground) on the other side of the screen to create “plant” and “no plant” treatments. Polyvinyl chloride (PVC) collars were installed in each mesocosm as a base for GHG sampling.

Hydrologic treatments were started two weeks after installation of PVC collars and the initiation of plant and no plant treatments. To manipulate hydrology, vinyl tubing connected to a one L water bottle was inserted on each side of the mesocosm, to a depth three cm from the bottom of the mesocosm container. Water levels inside the mesocosm were maintained by filling the one

L bottle to the desired height using rainwater collected from a cistern. Mesocosms exposed to wet conditions were flooded and maintained at maximum container height (18 cm). Mesocosms exposed to dry conditions were maintained at a five cm water level. Interim hydrologic treatment fluctuated between flooded and dry conditions every two weeks, starting with a wet treatment, and ending with a dry treatment. Experimental treatment lasted eight weeks, with 36 mesocosms evenly representing three levels of hydrologic history (dry, wet, interim), two levels of plant treatment (plant, no plant), and three levels of hydrologic treatment (dry, wet, interim) in a factorial experimental design (Figure 2).

Measuring Greenhouse Gases

We investigated the impact of hydrology and vegetation on GHG production, measuring GHG fluxes starting on June 13, 2016, two weeks after establishing hydrologic treatments, and continuing biweekly until August 11, 2016, for a total of five sampling events. GHG collection chambers, made from clear acrylic tubing, were 20 cm high with a diameter of 8.25 cm. Using clear chambers allowed us to capture total GHG fluxes, not just soil respiration due to microbial activity. Chambers were sealed with silicon and a cap fitted with a 33 mm septum as a gas sampling port. During sampling, the chambers were placed on preinstalled PVC collars and sealed with tape to prevent diffusion (45). Gas samples were collected at 30, 60, 120, and 180 minutes post-chamber attachment. Ambient (T0) samples were not collected before chamber closure but were later collected from the mesocosm incubation field site (ECU West Research Campus) as part of a 16-month GHG sampling effort, from August 2021 to December 2022. Monthly average ambient GHG concentrations were calculated and used as the T0 concentration for mesocosm flux timepoints in the corresponding month. All GHG samples were collected using a 20 mL syringe with a needle, mixing the headspace gas three times before collecting a 20 mL sample, then

splitting between a pair of three mL glass Exetainer vials (Lampeter, Wales, UK) with screw tops and dual-layer septa. Samples were stored upside down at room temperature in a dark location and analyzed within 96 hours.

We analyzed GHG concentrations with a Shimadzu gas chromatograph (GC-2014), equipped with an electron capture detector for nitrous oxide (N_2O) and a flame ionization detector with a methanizer for CH_4 and CO_2. Calibration standards for June 13 and June 28, 2016, contained 0, 120, 240, 360, and 480 parts per million (ppm) CO_2; 0, 1, 2, 3, 4, and 5 ppm CH_4; 0, 0.2, 0.4, 0.6, 0.8, and 1 ppm N_2O. Calibration standards for July 11, Jul 25, and August 11, 2016, contained 0, 120, 480, 1200, 2400, and 3000 ppm CO_2; 0, 1, 4, 20, 40, and 50 ppm CH_4; 0, 0.2, 0.8, 20, 40, and 50 ppm N_2O. Calibration standards for the ambient samples collected monthly from August 2021 to December 2022 contained 0, 120, 240, 360, 480, 600, 1200, 1800, 2400, and 3000 ppm CO_2; 0, 1, 2, 3, 4, 5, 10, 20, 30, 40, and 50 ppm CH_4; 0, 0.2, 0.4, 0.6, 0.8, 1, 10, 20, 30, 40, and 50 ppm N_2O. Samples exceeding the calibration curve were diluted and reanalyzed. GHG fluxes were calculated using the gasfluxes package implemented in the R Statistical Environment and RStudio (RStudio 2024.12.0+467, Rv4.4.2) (46, 47).

Amplicon and Shotgun Metagenomic Sequencing

Based on amplicon sequencing, we identified a subset of samples representing the most distinct microbial communities for shotgun metagenomic sequencing (48, 49). Briefly, we chose a set of baseline (before hydrologic/plant treatment) and post-flooding/drying treatment samples. Baseline samples were sourced from dry (water level at about -20 cm, n = 4) and wet (water level at about 0 cm, n = 4) hydrologic conditions, referred to as hydrologic history. At the end of the eight-week experiment, we selected a subset of samples from the hydrologic treatments (prolonged drying or wetting only) and plant treatments (presence or absence of vegetation) (n = 16). After

genomic DNA extraction using the Qiagen DNeasy PowerMax Soil Kit, samples were sent to the U.S. Department of Energy (DOE) Joint Genome Institute (JGI) for sequencing and analysis (GOLD study ID Gs0142547 and NCBI BioProject accession number PRJNA641216). Bin methods in the IMG pipeline (MetaBAT version 2.12.1, CheckM v1.0.12, GTDB database release 86, GTDB-tk version v0.2.2) were used to curate 14 medium- to high-quality bins from the metagenomes. Medium-quality bins have at least 50% completion, and less than 10% contamination. High quality bins have greater than 90% completion, less than 5% contamination, the presence of 23S, 16S, and 5S rRNA genes, and at least 18 tRNA genes (50). Description of sample processing and metagenomic sequencing can be found in Peralta et al. 2020 (48).

From the metagenomes, we curated functional gene sets using IMG/M's integrated Kyoto Encyclopedia of Genes and Genomes (KEGG) module list (51). We focused on the following four functional gene sets associated with S cycling: Assimilatory Sulfate Reduction (M00176), Dissimilatory Sulfate Reduction (M00596), Thiosulfate Oxidation by SOX Complex (M00595), and Sulfate-Sulfur Assimilation (M00616). We also analyzed KEGG module M00530: Dissimilatory Nitrate Reduction to Ammonia (DNRA). Previously, we examined metabolic gene modules related to biogenic GHG emissions, including Methanogen (M00617) (49). For a comparison of functional genes impacting CH_4 flux, we analyzed Methane Oxidation (M00174).

The IMG/M, and publicly available databases in general, have limited options for Fe gene analysis. From IMG/M's integrated TIGRFAM tool, we analyzed two genes putatively involved in Fe reduction: decaheme c-type cytochrome, OmcA/MtrC family (TIGR03507) and decaheme-associated outer membrane protein, MtrB/PioB family (TIGR03509). These two genes were analyzed together as one "module", analogous to collections of KEGG Orthologs (KOs) within each KEGG Module.

For further Fe gene analysis, we analyzed all metagenomes using FeGenie, a hidden Markov model (HMM) tool designed for the identification of Fe genes and Fe gene neighborhoods (52). Complete nucleotide assemblies (FNA files) for each metagenome were downloaded from IMG/MER, then searched using FeGenie's custom HMM scripts. Bitscores greater than the bitscore cuttoff were counted as positive "hits" for a given Fe gene. Counts of gene hits were totaled within each of FeGenie's gene categories: (1) iron acquisition (a. iron transport, b. heme transport, c. heme oxygenase, d. siderophore synthesis, e. siderophore transport, f. siderophore transport potential); (2) iron gene regulation; (3) iron oxidation; (4) possible iron oxidation and possible iron reduction; (5) probable iron reduction; (6) iron reduction; (7) iron storage; (8) magnetosome formation. Counts within each FeGenie category were then converted to relative abundance, and relative abundance matrices were then converted to Bray-Curtis distance matrices. Functional gene counts within each respective KEGG Module and TIGRfam "module", followed a similar process: conversion of counts to relative abundance (relative to module total counts), and conversion of relative abundance matrices to Bray-Curtis matrices.

Measuring Integrated Soil Redox Status

Soil redox status was measured using Indicator of Reduction in Soils (IRIS) tubes, following the methodology described in our previous study (49, 53). At the beginning of the experiment, two IRIS tubes were installed in each mesocosm: one on the plant side and one on the bare soil ("no plant") side. The tubes were incubated for two weeks before removal and analysis. A non-coated PVC pipe was used to fill the hole left by the removed IRIS tube. Two weeks prior to the end of the experiment, the non-coated PVC pipe was replaced with a new IRIS tube to measure soil redox status at the end of the experiment.

The surface area of Fe(III) paint removed from the IRIS tubes was quantified using ImageJ (54). The percentage of paint removed was used to interpret redox status, with higher percentages indicating more reducing conditions. For further details, please refer to Bledsoe et al. (2024).

Measuring Soil Factors

Soil proprieties were determined from soils collected during the destructive sampling of mesocosms at the end of the experiment. A sample of air-dried soil from each mesocosm was sent to Waters Agricultural Laboratories, Inc. (Warsaw, NC) and analyzed for pH, phosphorus, potassium, magnesium, sulfur, manganese, iron, and humic matter, using standard Mehlich III methods (55).

Statistical Analyses

All statistical analyses were performed in the R statistical environment (RStudio 2024.12.0+467, Rv4.4.2) (46). We found GHG and IRIS tube data to be non-Gaussian, and to have extreme outliers. To address these extreme outliers and non-normal data distribution, we employed nonparametric statistical methods to assess differences in GHG fluxes and IRIS percent across hydrologic treatments. For differences in GHG fluxes and IRIS percent among the three hydrologic treatments (dry, interim, and wet), we used Kruskal-Wallis Rank Sum tests, grouped by sampling date to accommodate repeated measures. When the Kruskal-Wallis test indicated significant differences among treatment groups for a given sampling date ($p \leq 0.05$), we conducted pairwise comparisons using the Dwass, Steel, Critchlow, and Fligner (SDCFlig) test using the function pSDCFlig in the package NSM3 (46, 56). We visualized bacterial community responses to hydrologic history (field conditions), hydrologic treatment (contemporary dry/wet treatments), and plant presence/absence using the ordination method, principal coordinates analysis (PCoA), of bacterial community composition based on Bray-Curtis dissimilarity. We also used PCoA to

visualize the composition of functional gene categories, separating points by hydrologic history, hydrologic treatment, and plant presence/absence. We used permutational multivariate analysis of variance (PERMANOVA) to measure the variation in bacterial community composition due to hydrologic history, hydrologic treatment, and plant presence. Hypothesis testing using PERMANOVA was performed using the vegan::adonis function (57). Finally, soil parameters and GHG fluxes were compared against bacterial community and functional patterns (based on Bray-Curtis dissimilarity) using the vegan::envfit function (57). The GHG fluxes and soil parameters with envfit $p \leq 0.05$ were plotted as vectors, scaled by their correlation, on PCoA plots of functional gene composition. Distance-based partial least squares regression (DBPLSR) was used to measure relationships between Bray-Curtis distance matrices and GHG fluxes.

Next, we conducted a series of Mantel tests to measure correlations between Bray-Curtis distance matrices. We assessed the potential for NO_3^--driven SO_4^{2-} production by testing the distance matrix correlations between the composition of NO_3^- reduction pathways (denitrification and DNRA) and the composition of thiosulfate oxidation by the SOX complex. We conducted a Mantel test for each respective NO_3^- reduction pathway (denitrification and DNRA) correlated to thiosulfate oxidation by the SOX complex. We ran a series of Mantel tests for pairs of SO_4^{2-} reduction and Fe reduction distance matrices: Fe reduction ~ SO_4^{2-} reduction (assimilatory and dissimilatory), Fe reduction ~ assimilatory SO_4^{2-} reduction, and Fe reduction ~ dissimilatory SO_4^{2-} reduction. To investigate correlations between SO_4^{2-} and Fe reduction under different hydrological conditions, the SO_4^{2} reduction (assimilatory and dissimilatory) and Fe reduction modules were subset by hydrologic history (wet or dry) and hydrologic treatment (wet or dry). We evaluated the strength of Mantel r correlations between pairs of SO_4^{2-} reduction and Fe reduction distance

matrices within each hydrologic condition (e.g., wet hydrologic history) and used a statistical cutoff of $p \leq 0.05$.

Data Availability

All code and data used in this study are in a public GitHub repository (https://github.com/PeraltaLab/WetlandMesocosm_GHG_Timberlake) with a Zenodo DOI (10.5281/zenodo.4042109 (to be updated)). Raw amplicon sequence files can be found at NCBI SRA BioProject ID PRJNA636184, and metagenome sequence files can be found at NCBI SRA BioProject ID PRJNA641216.

RESULTS

Using a wetland mesocosm approach, we tested the following hypotheses: (i) in oxidizing conditions (dry and/or plant presence) SO_4^{2-} reduction and Fe reduction will not be linked/coupled, where coupled means a significant correlation between Bray-Curtis distance matrices of SO_4^{2-} reduction and Fe reduction; and (ii) in reducing conditions (wet and/or plant absence) coupling between SO_4^{2-} reduction and Fe reduction will be observed, and these processes will contribute to CO_2 production (fit with CO_2 fluxes using envfit) while competing with methanogenesis (observed as negative relationship with methanogenic functional genes and CH_4 fluxes). The eight-week hydrologic manipulation resulted in differences in soil redox status based on the percent of paint removed from IRIS tubes (IRIS percent) during the week zero and week eight timepoints measured at the start and end of the mesocosm incubation. During week zero, which followed two weeks of initial plant and hydrologic treatment and IRIS tube incubation, both interim and wet treatments exhibited more reducing conditions than the dry treatment (SDCFlig $p \leq 0.05$; Figure 3). At the end of the eight-week experiment, the wet treatment displayed reducing conditions while the dry and interim treatments were not reducing (Figure 3).

Greenhouse Gas Fluxes

Here, we highlight general trends in GHG fluxes. A more detailed analysis of the GHG data is presented in Bledsoe et al. 2024 (49). The GHG fluxes varied over five timepoints collected every two weeks during the eight-week experiment. While the CH_4 fluxes were generally greater in wet vs. dry treatment, CH_4 fluxes were similar across treatments in the first and final timepoints (Figure 4). The CO_2 fluxes were greater in dry mesocosms, and no plant vs plant mesocosms, and the N_2O fluxes were near zero and similar across treatments for most of the eight-week experiment (Figure 4).

Sulfur Functional Genes

We measured how hydrology and plant presence influenced the community composition of S cycling genes. Hydrologic treatment strongly influenced the composition of SO_4^{2-}-S assimilation (PERMANOVA, $F_{1, 23} = 3.917$, $R^2 = 0.144$, $p = 0.008$; Table 1; Appendix S1: Table A1) and assimilatory SO_4^{2-} reduction functional genes (PERMANOVA, $F_{1, 23} = 4.111$, $R^2 = 0.156$, $p = 0.013$; Table 1; Appendix S1: Table A1). The response of SO_4^{2-}-S assimilation and assimilatory SO_4^{2-} reduction gene composition correlated to redox status measured as the percent paint removed from IRIS tubes (sulfate assimilation-IRIS envfit, $R^2 = 0.285$, $p = 0.032$, Figure 5A; assimilatory sulfate reduction-IRIS envfit, $R^2 = 0.301$, $p = 0.027$, Figure 5B). Hydrologic history strongly influenced the compositions of dissimilatory SO_4^{2-} reduction (PERMANOVA, $F_{1, 23} = 10.397$, $R^2 = 0.316$, $p = 0.0003$; Table 1; Appendix S1: Table A1) and thiosulfate oxidation by the SOX complex (PERMANOVA, $F_{1, 23} = 6.547$, $R^2 = 0.243$, $p = 0.009$; Table 1; Appendix S1: Table A1). The combination of assimilatory and dissimilatory SO_4^{2-} reduction differed in composition according to hydrologic history and treatment (PERMANOVA, history: $F_{1, 23} = 2.830$, $R^2 = 0.108$, $p = 0.030$, treatment: $F_{1, 23} = 2.906$, $R^2 = 0.111$, $p = 0.026$; Table 1; Appendix S1: Table A1). The community composition of SO_4^{2-} reduction (assimilatory and dissimilatory) correlated significantly with percent soil moisture (envfit, $R^2 = 0.298$, $p = 0.023$; Figure 6C). The composition of dissimilatory sulfate reduction genes differed according to hydrologic history (PERMANOVA, history: $F_{1, 23} = 10.397$, $R^2 = 0.316$, $p = 0.0003$; Table 1; Appendix S1: Table A1), and was related to CH_4 flux (envfit, $R^2 = 0.401$, $p = 0.003$; Figure 5C; Figure 7). Based on DBPLSR, the percent of variance in CH_4 flux explained by dissimilatory SO_4^{2-} reduction decreased by 12% from week zero to week eight (adjusted $R^2_{Week\ 0} = 0.68$, adjusted $R^2_{Week\ 8} = 0.56$, based on components 1 and 2; Figure 7; Appendix S1: Table A2). Functional genes for methane oxidation and methanogenesis

explained less variance in methane fluxes than dissimilatory SO_4^- reduction functional gene composition (Figure 7; Appendix S1: Table A2). The relationship between CH_4 fluxes and methane oxidation increased in strength over the course of the experiment, and that of methanogenesis decreased from week zero to week eight (Figure 7; Appendix S1: Table A2).

Nitrate-Driven Sulfate Production

To evaluate linkages between NO_3^- reduction and sulfide oxidation, we measured the extent to which metabolic gene composition of NO_3^- reduction pathways (denitrification and DNRA) related to thiosulfate oxidation. Based on a cutoff of $\alpha = 0.05$, the composition of DNRA genes was significantly correlated with thiosulfate oxidation by SOX complex (Mantel $r = 0.196$, $p = 0.0499$; Appendix S1: Table A3), and denitrification gene composition was not correlated with thiosulfate oxidation by SOX complex (Mantel $r = 0.117$, $p = 0.170$; Appendix S1: Table A3), but correlation coefficients were similar for both NO_3^- reduction pathways.

Iron Functional Genes

The composition of all Fe-active genes, and the composition of Fe reduction genes, were used to evaluate the response of Fe cycling communities from different hydrologic histories to flooding/drying and plant presence/absence. Hydrologic history influenced the composition of all Fe genes identified by FeGenie (PERMANOVA: $F_{1, 23} = 4.173$, $R^2 = 0.185$, $p = 0.031$; Table 1; Appendix S1: Table A1). The composition of Fe reduction genes identified by FeGenie also diverged according to history (PERMANOVA: $F_{1, 23} = 3.358$, $R^2 = 0.132$, $p = 0.004$; Table 1; Appendix S1: Table A1), while the composition of Fe reduction genes based on TIGRFAMS mtrBC differed by plant presence/absence and treatment (PERMANOVA, plant: $F_{2, 23} = 9.967$, $R^2 = 0.335$, $p = 0.002$, treatment: $F_{1, 23} = 19.012$, $R^2 = 0.319$, p = 0.00069; Table 1; Appendix S1: Table A1).

Sulfate Reduction and Iron Reduction

We observed a significant correlation between the composition of functional genes associated with Fe reduction and assimilatory SO_4^{2-} reduction (Mantel r = 0.222, p = 0.008; Appendix S1: Table A3). Similarly, results showed a significant correlation between functional gene composition of Fe reduction and dissimilatory SO_4^{2-} reduction (Mantel r = 0.313, p = 0.006; Appendix S1: Table A3). However, results showed no correlation when assimilatory and dissimilatory SO_4^{2-} reduction were combined into a single module and compared to Fe reduction (Mantel r = 0.064, p = 0.249; Appendix S1: Table A3). Then, we assessed correlations between SO_4^{2-} and Fe reduction under different hydrologic conditions. In the wet history, dry history, and dry treatment, there were no significant correlations between SO_4^{2-} reduction and Fe reduction (Appendix S1: Table A4). In the wet treatment, there was a significant correlation between functional gene composition of SO_4^{2-} reduction and Fe reduction (Mantel r = 0.360, p = 0.010; Appendix S1: Table A4).

Metagenome Bins

Binning methods in the IMG pipeline resulted in 14 medium- to high-quality metagenome bins (Appendix S1; Table A5). Except for one bin attributed to an Archaeal lineage (*Nitrosotalea*), all other bins were identified as bacterial taxa (Appendix S1; Table A5). The bins were sourced from varying hydrologic histories, hydrologic treatments, and plant presence/absence treatments. We found genes for dissimilatory SO_4^{2-} reduction and/or Fe reduction in all but four of the metagenome bins (Figure 8). Bins corresponding to *Burkholderiaceae bacterium JOSHI-001* were found in both wet and dry history (Figure 8). The *JOSHI-001* bin from dry hydrologic history had a more complete dissimilatory SO_4^{2-} reduction pathway than the *JOSHI-001* bin from wet

hydrologic history (Figure 8). But the wet history *JOSHI-001* bin had both *mtrB* and *mtrC* (Fe reduction) while the dry history *JOSHI-001* bin only contained one copy of *mtrC* (Figure 8).

We also surveyed the metagenome bins for functional genes related to methanogenesis and methane oxidation. Hits for at least one methanogenic functional gene were found in all 14 metagenome bins, but only one hit for a methane oxidation gene (*pmoA-amoA*) was found in the *Nitrosotalea* bin (Figure 8).

DISCUSSION

Wetland soil Fe availability, hydrologic conditions, and plant-microbe interactions mediate the impacts of SWISLR on coastal freshwater wetlands (11, 14, 15). In this study, we used a mesocosm approach to examine the effects of hydrologic conditions and plant presence/absence on soils sourced from varying hydrologic histories (wet and dry). We found that hydrologic history (wet vs dry) influenced the composition of genes involved in dissimilatory SO_4^{2-} reduction, thiosulfate oxidation, and Fe reduction. The eight-week hydrologic manipulation also modified the community composition of assimilatory SO_4^{2-} reduction genes and resulted in correlated SO_4^{2-} reduction and Fe reduction gene compositions in the wet hydrologic treatment. The S and Fe gene modules were linked with C and N cycling; specifically, DNRA and thiosulfate oxidation gene compositions correlated, and dissimilatory SO_4^{2-} reduction gene composition explained variance in CH_4 fluxes. These results indicate that historical conditions strongly influence the magnitude of soil microbial community responses to contemporary changes in hydrologic conditions and plant cover.

Past and Current Hydrologic Conditions Influence Sulfur Functional Genes

The influence of hydrologic conditions, both historical and during the eight-week contemporary hydrologic treatments, was evident in the composition of S-related gene modules. The community-level compositions of SO_4^{2-}-S assimilation and assimilatory SO_4^{2-} reduction genes both differed by hydrologic treatment, while the compositions of dissimilatory SO_4^{2-} reduction and thiosulfate oxidation by the SOX complex both differed by hydrologic history (Table 1; Appendix S1: Table A1). The composition of SO_4^{2-} reduction functional genes (assimilatory and dissimilatory) correlated with percent soil moisture (Figure 6C). This relationship revealed the importance of hydrology in SO_4^{2-} reduction gene composition.

The influence of hydrologic history on S metabolism in this coastal wetland soil is potentially two-fold: the introduction of SO_4^{2-} via saltwater intrusion, and the reducing conditions found in waterlogged soils (in wet history), compared to more oxidizing conditions found in drier conditions (at a greater elevation above the water table). In previous work, Ardón and colleagues (2013) found evidence of saltwater intrusion via surface water at TOWeR. There is potential for drought-induced saltwater intrusion at this site, where the surrounding estuary's salinity increases during drought, and winds or tides transport the brackish water upstream to the TOWeR site (14). Flooding during storm surges is another mechanism by which surface water can facilitate saltwater intrusion (58). Saltwater intrusion via either mechanism, drought or storm surge, deposits SO_4^{2-} in the soil (14, 15). This SO_4^{2-} influx could persist in the soil and be internally transformed to other S species (sulfite, thiosulfate, sulfide, S^0) (15, 59, 60).

Because the S from saltwater can persist in the soil, changes in soil O_2 availability due to precipitation or dry down are important for structuring anaerobic and aerobic S metabolisms following the saltwater intrusion event (15). Assimilatory SO_4^{2-} reduction is a highly conserved process, used by both aerobic and anaerobic organisms (60). On the other hand, a subset of anaerobic microorganisms participate in dissimilatory SO_4^{2-} reduction (60). Both assimilatory and dissimilatory SO_4^{2-} reduction produce hydrogen sulfide (H_2S) (60). In assimilatory SO_4^{2-} reduction, H_2S is produced as an intermediate that is incorporated into biomolecules (60). In contrast, dissimilatory SO_4^{2-} reduction produces H_2S as a waste product, in larger quantities than assimilatory SO_4^{2-} reduction, and is therefore, a more important metabolism to consider during freshwater ecosystem sulfidization events (12, 15, 60).

While SO_4^{2-} reduction described above consumes SO_4^{2-}, thiosulfate oxidation by the SOX complex produces SO_4^{2-} (59, 60). Phototrophs, mixotrophs, and heterotrophs participate in

thiosulfate oxidation via the SOX complex in a variety of assimilatory, dissimilatory, aerobic, and anaerobic pathways (59). In the context of a microbial community, thiosulfate oxidation (and S oxidation pathways in general) is important for regenerating oxidized S species (i.e., SO_4^{2-}) that can again be reduced by SRM (59). In the current study, hydrologic history influenced the composition of thiosulfate oxidation by SOX complex genes, but it is not clear which historical conditions (i.e., wet or dry) favored thiosulfate oxidation (Table 1; Appendix S1: Table A1).

A variety of electron acceptors can be used in the oxidation of thiosulfate (59). In freshwater wetlands in Michigan, NO_3^- reduction contributed to SO_4^{2-} production via oxidation of sulfide (40). Of the two major NO_3^- reduction pathways, denitrification and DNRA, S-driven denitrification made up a greater fraction of NO_3^- removal, but S-driven DNRA also contributed significantly to NO_3^- removal (40). In the estuarine landscape, sulfide oxidation can increase sediment O_2 demand, and sediment O_2 demand was found to be positively correlated with N_2 flux (primarily denitrification with low potential DNRA) (61). To test for NO_3^--driven SO_4^{2-} production in our mesocosm experiment, we measured correlations between the Bray-Curtis distance matrices of denitrification genes and thiosulfate oxidation genes, and DNRA genes and thiosulfate oxidation genes. While correlation coefficients for both NO_3^- reduction pathways were similarly low, we found that DNRA was significantly correlated to thiosulfate oxidation by SOX complex (Mantel $r = 0.196$, $p = 0.0499$; Appendix S1: Table A3), but denitrification was not correlated to thiosulfate oxidation by SOX complex (Mantel $r = 0.117$, $p = 0.170$; Appendix S1: Table A3). Our DNA-based approach indicated differences in the strengths of associations between functional gene modules that would require further evaluation of gene expression and biogeochemical transformations to reveal the differences in NO_3^- and SO_4^{2-} concentrations linked with DNRA vs. denitrification functions.

It is difficult to predict the balance of denitrification and DNRA in a given system, but some evidence supports the importance of NO_3^- loading and the oxidation state of S sources (62–64). Interestingly, Li and colleagues (2022) found thiosulfate oxidation to be strongly coupled with denitrification, but not at all coupled with DNRA (64). It is possible that in the thiosulfate enrichment incubation experiment performed by Li and colleagues (2022), denitrifying microorganisms outcompeted DNRA bacteria by rapidly consuming added thiosulfate (64). It is unclear whether Li and colleagues' results showed an inability of DNRA bacteria to use thiosulfate as an electron donor, or if denitrifiers directly outcompeted DNRA bacteria for thiosulfate (64). Further work is required to understand the connections between DNRA and thiosulfate oxidation in coastal wetlands.

Hydrologic History Influences Iron Functional Gene Composition

Hydrologic history modified Fe functional gene composition. Specifically, hydrologic history altered the composition of all Fe genes identified by FeGenie and the subset of Fe reduction genes identified by FeGenie (Table 1; Appendix S1: Table A1). Transformations of Fe vary based on the redox status and pH of the environment (42). It follows that dry or wet, and oxic or anoxic historical conditions would structure different Fe cycling communities. In anoxic environments (with pH > 4), microbial Fe(III) reduction is a major electron sink for organic matter oxidation (42, 65). Therefore, greater genetic potential for Fe reduction may exist in historically wet soils with presumably lower O_2 availability. But this inference is complicated by the ongoing microbial transformations of N alongside aerobic and anaerobic oxidations and reductions of Fe (reviewed in Weber et al., 2006). Our analysis of the composition of all Fe genes identified by FeGenie highlights the impact of hydrologic history on Fe cycling, and Fe reduction specifically.

The FeGenie tool was developed in response to a lack of Fe annotation tools (52). Prior to FeGenie, one of the few options for identifying Fe reduction genes was TIGRFAMS *mtrB* (TIGR03509) and *mtrC* (TIGR03507) (52). We also used the composition of TIGR03509 and TIGR03507 to analyze genetic potential for Fe reduction and found the composition to differ by plant (presence/absence) and hydrologic treatment (Table 1; Appendix S1: Table A1). The genes *mtrB* and *mtrC* are included in FeGenie, but FeGenie and IMG's TIGRFAM annotation pipeline resulted in different counts of *mtrB* and *mtrC*. These contrasting results from different annotation tools highlight the current uncertainties in Fe gene annotation and point towards a need for increased consensus in Fe gene annotation.

Sulfate Reduction and Iron Reduction Correlate in Reducing Conditions

We hypothesized that SO_4^{2-} reduction and Fe reduction would be coupled (meaning significantly correlated) in reducing (i.e., flooded) conditions. We found that the functional gene composition of SO_4^{2-} reduction and Fe reduction genes were significantly correlated in the wet treatment, but not in the wet history, or either of dry hydrologic treatment or history (Appendix S1: Table A4). This indicates that the functional gene composition of both metabolisms responded similarly and strongly to eight weeks of flooding. Because the association was based on DNA sequencing, it indicates that the relative abundances of SRM and FeRM changed in response to hydrologic treatment over eight weeks of incubation but does not reflect the rates of SO_4^{2-} reduction and Fe reduction. Both SO_4^{2-} reduction and Fe reduction are metabolisms commonly found in anoxic sediments (66). The wet treatment appears to have imposed suboxic/anoxic conditions, characterized by a higher percent of paint removed from IRIS tubes (Figure 3), and these reducing conditions were likely conducive to both SRM and FeRM. This supports previous findings of correlated SO_4^{2-} and Fe reduction in TOWeR soils (15).

Dissimilatory Sulfate Reduction Gene Composition Explains Variance in Methane Fluxes

In addition to the Fe-S linkages described above, dissimilatory SO_4^{2-} reduction gene composition was related to production of CH_4. Dissimilatory SO_4^{2-} reduction gene composition was significantly correlated with CH_4 fluxes (Figures 5C and 7). At the start of the experiment (week zero), the composition of dissimilatory SO_4^{2-} reduction genes had a stronger relationship with CH_4 fluxes than either CH_4 oxidation or methanogenesis functional genes (Figure 7, Appendix S1: Table A2). At the end of the experiment, dissimilatory SO_4^{2-} reduction still explained a greater percentage of variance in CH_4 fluxes than methanogenesis, but less than CH_4 oxidation (Figure 7, Appendix S1: Table A2). The CH_4 oxidation gene composition increased in importance from week zero to week eight, but no treatment impacts on CH_4 oxidation gene composition were observed (Appendix S1: Table A1). In general, CH_4 fluxes decreased over the course of the experiment (Figure 4), likely explaining the decrease in the strength of the relationship between CH_4 fluxes and methanogenesis gene composition from week zero to week eight (Figure 7, Appendix S1: Table A2). The relationship between CH_4 fluxes and dissimilatory SO_4^{2-} reduction genes mirrored that of methanogen gene composition, dropping from week zero to week eight, but was higher for dissimilatory SO_4^{2-} reduction at both timepoints. This caused us to question whether the relationship between methanogens and SRM was mutualistic, competitive, or covarying with hydrologic conditions.

Our compositional approach showed that variation in dissimilatory SO_4^{2-} reduction gene composition corresponded with variance in CH_4 fluxes but does not reveal linear relationships between gene abundance and CH_4 fluxes. Therefore, relationships between dissimilatory SO_4^{2-} reduction and CH_4 fluxes could be positive (increased gene abundance with increased CH_4 fluxes) or negative (increased gene abundance with decreased CH_4 fluxes, or vice-versa). While Fe

reduction gene composition was not strongly related to CH_4 fluxes, it was correlated with SO_4 reduction gene composition (Appendix S1; Tables A3 and A4). Iron reduction is known to inhibit methanogenesis through substrate competition (acetate and hydrogen), both between separate groups of FeRM and methanogens capable of Fe reduction (67, 68). Ferric iron compounds have also been shown to directly inhibit methanogenesis (68). The interactions among dissimilatory SO_4^{2-} reduction, Fe reduction, and methanogenesis are complex and may structure ecosystem-level transformations of S, Fe, and C.

Explanations for both positive and negative relationships between SO_4^{2-} and Fe reduction genes and CH_4 fluxes are possible. Dissimilatory SO_4^{2-} reduction, Fe reduction, and methanogenesis are all generally considered anaerobic metabolisms (66, 69). Therefore, the reducing or oxidizing environment (e.g., wet vs. dry conditions) could have impacted all three metabolisms similarly, resulting in the observed correlations. Alternatively, the correlation between dissimilatory SO_4^{2-} reduction and CH_4 fluxes could be the result of competition between microbial taxa. Since Fe reduction and dissimilatory SO_4^{2-} reduction are more thermodynamically favorable than methanogenesis (in standard conditions) (21), it is conceivable that when FeRM and SRM are abundant (because Fe(III) and SO_4^{2-} are available), these microbial communities outcompete the less abundant methanogens, resulting in a negative correlation. Similarly, methanogenic archaea may switch from methanogenesis to Fe reduction when resources allow (70), and the presence of Fe reduction and methanogenic functional genes in three metagenome bins indicates genetic potential for this switch, but none of the bins were assigned to methanogenic lineages (Figure 8). The specific resources that methanogens and SRM compete for are acetate and hydrogen (71–73). Methylotrophic methanogens avoid competition with SRM by consuming methyl compounds that are not consumed by SRM (74, 75). In a recent study, Bueno de Mesquita

and colleagues incubated TOWeR soils with artificial seawater, with and without SO_4^{2-}, but found no increase in methyl-reducing methanogens, indicating that avoiding competition with SRM during a pulse of SO_4^{2-} availability was not a widely adopted strategy by the TOWeR methanogen community (76). A shift in methanogen community composition may require more than 12 weeks to develop, and similarly in our eight-week experiment, slow growing methanogens may have been unable to adapt to changing hydrologic conditions to create a significant shift in methanogen functional gene abundance. In addition to substrate competition, SO_4^{2-} reduction may directly inhibit methanogenesis through the production of sulfide, but some methanogens can tolerate high sulfide concentrations (77–79). Given that both dissimilatory SO_4^{2-} reduction and methanogenesis functional genes decreased in their ability to explain variance in CH_4 fluxes from start to end of the experiment (Figure 7), competition or inhibition between the two functional groups is not well supported by our data. Instead, mutualism may explain the concomitant shifts in variance explained in CH_4 fluxes, and the strong relationship between dissimilatory SO_4^{2-} reduction and CH_4 fluxes (Figures 5C, 7). A known mutualism between SRM and methanogens exists, in which methanogens consume H_2S produced by SRM, and thereby maintain the required pH for both SO_4^{2-} reduction and methanogenesis to proceed (80). Relationships between SRM and methanogens vary between environments and experimental setups and seem especially tied to C substrate and sulfide concentrations. Our functional gene analysis based on metagenomic sequencing and *in situ* CH_4 fluxes supports a mutualistic, or environmentally co-varying relationship between SRM and methanogens. To consistently predict freshwater wetland CH_4 emissions under future SWISLR, experiments that isolate the impact of SO_4^{2-} on CH_4 emissions (like Bueno de Mesquita et al., 2024), will need to be replicated in a range of freshwater wetland soils.

CONCLUSION

An oversimplified view of biogeochemistry might describe the biogeochemical cycles of C, N, Fe, and S in isolation, with transformations structured in communities according to thermodynamic favorability (26, 81). But it is increasingly clear that biogeochemical cycles are intertwined, and a "microbial energy economy" that relies on resource availability and biotic and abiotic interactions is closer to reality than a hierarchically structured thermodynamic ladder (19, 81). The specific biotic and abiotic context in which communities are found will likely determine which linkages between cycles are relevant. In the wetland soil mesocosm study presented here, Fe-rich soils and seasonal saltwater intrusion importing SO_4^{2-} make Fe and S linkages with C and N metabolism particularly relevant. Considering linked biogeochemical cycles, and the historical context-dependence of an ecosystem will help improve predictions of the future impacts of SWISLR on coastal biogeochemistry.

ACKNOWLEDGMENTS

Thank you to R. Bledsoe for developing and executing the experiment. We extend our gratitude to J. LeCrone, L. Armstrong, M. Stillwagon, G. Gunderson, C. Eakins, J. Basco, and C. Bledsoe for their invaluable assistance in the field and laboratory. We also appreciate J. Gill and the East Carolina University grounds crew for their efforts in maintaining the area around the shade house. Additionally, we thank M. Muscarella for contributing to the microbiome analyses. Thank you to J. Hoben and E. Field for manuscript revisions and analysis ideas. E. Field and C. Joyner helped with FeGenie troubleshooting and shared computing resources. This research was funded by the National Science Foundation, through a Graduate Research Fellowship Program (GRFP) grant

awarded to R.B.B., grant no. DGE-2125684 to C.G.F., and grants DEB #1845845 and CNH2 #2009185 awarded to A.L.P. The metagenomes were generated by the DOE Joint Genome Institute (JGI) under the Community Science Program (CSP) grant 503952. The work at the DOE JGI, a DOE Office of Science User Facility, is supported under contract DE-AC02-05CH11231.

REFERENCES

1. Jordan SJ, Stoffer J, Nestlerode JA. 2011. Wetlands as Sinks for Reactive Nitrogen at Continental and Global Scales: A Meta-Analysis. Ecosystems 14:144–155.

2. Kayranli B, Scholz M, Mustafa A, Hedmark Å. 2010. Carbon Storage and Fluxes within Freshwater Wetlands: a Critical Review. Wetlands 30:111–124.

3. Nahlik AM, Fennessy MS. 2016. Carbon storage in US wetlands. Nat Commun 7:13835.

4. Widney SE, Smith D, Herbert ER, Schubauer-Berigan JP, Li F, Pennings SC, Craft CB. 2019. Chronic but not acute saltwater intrusion leads to large release of inorganic N in a tidal freshwater marsh. Science of The Total Environment 695:133779.

5. Neubauer SC, Piehler MF, Smyth AR, Franklin RB. 2019. Saltwater Intrusion Modifies Microbial Community Structure and Decreases Denitrification in Tidal Freshwater Marshes. Ecosystems 22:912–928.

6. Hopkinson CS, Cai W-J, Hu X. 2012. Carbon sequestration in wetland dominated coastal systems — a global sink of rapidly diminishing magnitude. Current Opinion in Environmental Sustainability 4:186–194.

7. Wilson BJ, Servais S, Charles SP, Davis SE, Gaiser EE, Kominoski JS, Richards JH, Troxler TG. 2018. Declines in Plant Productivity Drive Carbon Loss from Brackish Coastal Wetland Mesocosms Exposed to Saltwater Intrusion. Estuaries and Coasts 41:2147–2158.

8. Liu H, Jin Q, Xu X, Yang W, Fujiabayashi M, Luo J, Li Z, Zhou C, Shu P, Li W. 2025. Alteration of nitrogen sink and emission by vegetation distribution in a wetland with significant change in water level. Journal of Environmental Management 373:123920.

9. Wang T, Deng Z, Zhang C, Zou Y, Xie Y, Li F, Xiao F, Peng C. 2024. Vegetation types and flood water level are dominant factors controlling the carbon sequestration potential in Dongting Lake floodplain, China. Science of The Total Environment 921:171146.

10. Chu X, Han G, Xing Q, Xia J, Sun B, Li X, Yu J, Li D, Song W. 2019. Changes in plant biomass induced by soil moisture variability drive interannual variation in the net ecosystem CO2 exchange over a reclaimed coastal wetland. Agricultural and Forest Meteorology 264:138–148.

11. Herbert ER, Boon P, Burgin AJ, Neubauer SC, Franklin RB, Ardón M, Hopfensperger KN, Lamers LPM, Gell P. 2015. A global perspective on wetland salinization: ecological consequences of a growing threat to freshwater wetlands. Ecosphere 6:206.

12. Hopfensperger KN, Burgin AJ, Schoepfer VA, Helton AM. 2014. Impacts of Saltwater Incursion on Plant Communities, Anaerobic Microbial Metabolism, and Resulting Relationships in a Restored Freshwater Wetland. Ecosystems 17:792–807.

13. Kozlowski TT. 1984. Plant Responses to Flooding of Soil. BioScience 34:162–167.

14. Ardón M, Morse JL, Colman BP, Bernhardt ES. 2013. Drought-induced saltwater incursion leads to increased wetland nitrogen export. Global Change Biology 19:2976–2985.

15. Schoepfer VA, Bernhardt ES, Burgin AJ. 2014. Iron clad wetlands: Soil iron-sulfur buffering determines coastal wetland response to salt water incursion. Journal of Geophysical Research: Biogeosciences 119:2209–2219.

16. Johnson NW, Pastor J, Swain EB. 2019. Cumulative Sulfate Loads Shift Porewater to Sulfidic Conditions in Freshwater Wetland Sediment. Environmental Toxicology and Chemistry 38:1231–1244.

17. Li Y, Hua J, He C, Wang D, Zhao Z, Wang F, Wang Y, Wang X, Chen X, Liu X. 2024. Spartina alterniflora raised sediment sulfide in a tidal environment and buffered it with iron in the Jiuduansha Wetland. J Soils Sediments 24:657–669.

18. Intergovernmental Panel on Climate Change (IPCC). 2023. Climate Change 2022 – Impacts, Adaptation and Vulnerability: Working Group II Contribution to the Sixth Assessment Report of the Intergovernmental Panel on Climate Change.

19. Burgin AJ, Yang WH, Hamilton SK, Silver WL. 2011. Beyond carbon and nitrogen: how the microbial energy economy couples elemental cycles in diverse ecosystems. Frontiers in Ecology and the Environment 9:44–52.

20. Glass JB, Elbon CE, Williams LD. 2022. Something old, something new, something borrowed, something blue: the anaerobic microbial ancestry of aerobic respiration. Trends in Microbiology 0.

21. Wang X-N, Sun G-X, Zhu Y-G. 2017. Thermodynamic energy of anaerobic microbial redox reactions couples elemental biogeochemical cycles. J Soils Sediments 17:2831–2846.

22. DeAngelis KM, Silver WL, Thompson AW, Firestone MK. 2010. Microbial communities acclimate to recurring changes in soil redox potential status. Environmental Microbiology 12:3137–3149.

23. Peralta AL, Ludmer S, Matthews JW, Kent AD. 2014. Bacterial community response to changes in soil redox potential along a moisture gradient in restored wetlands. Ecological Engineering 73:246–253.

24. Crowther TW, van den Hoogen J, Wan J, Mayes MA, Keiser AD, Mo L, Averill C, Maynard DS. 2019. The global soil community and its influence on biogeochemistry. Science 365:550.

25. Falkowski PG, Fenchel T, Delong EF. 2008. The Microbial Engines That Drive Earth's Biogeochemical Cycles. Science 320:1034–1039.

26. Schlesinger WH, Cole JJ, Finzi AC, Holland EA. 2011. Introduction to coupled biogeochemical cycles. Frontiers in Ecology and the Environment 9:5–8.

27. Quince C, Walker AW, Simpson JT, Loman NJ, Segata N. 2017. Shotgun metagenomics, from sampling to analysis. 9. Nat Biotechnol 35:833–844.

28. Toole DR, Zhao J, Martens-Habbena W, Strauss SL. 2021. Bacterial functional prediction tools detect but underestimate metabolic diversity compared to shotgun metagenomics in southwest Florida soils. Applied Soil Ecology 168:104129.

29. Pezeshki SR, DeLaune RD. 2012. Soil Oxidation-Reduction in Wetlands and Its Impact on Plant Functioning. 2. Biology 1:196–221.

30. Patrick Jr. WH, Jugsujinda A. 1992. Sequential Reduction and Oxidation of Inorganic Nitrogen, Manganese, and Iron in Flooded Soil. Soil Science Society of America Journal 56:1071–1073.

31. RoyChowdhury T, Bramer L, Hoyt DW, Kim Y-M, Metz TO, McCue LA, Diefenderfer HL, Jansson JK, Bailey V. 2018. Temporal dynamics of CO2 and CH4 loss potentials in response to rapid hydrological shifts in tidal freshwater wetland soils. Ecological Engineering 114:104–114.

32. Chilton D, Hamilton DP, Nagelkerken I, Cook P, Hipsey MR, Reid R, Sheaves M, Waltham NJ, Brookes J. 2021. Environmental Flow Requirements of Estuaries: Providing Resilience to Current and Future Climate and Direct Anthropogenic Changes. Frontiers in Environmental Science 9.

33. Conley DJ, Paerl HW, Howarth RW, Boesch DF, Seitzinger SP, Havens KE, Lancelot C, Likens GE. 2009. Controlling Eutrophication: Nitrogen and Phosphorus. Science 323:1014–1015.

34. Kuypers MMM, Marchant HK, Kartal B. 2018. The microbial nitrogen-cycling network. 5. Nat Rev Microbiol 16:263–276.

35. Wallenstein MD, Myrold DD, Firestone M, Voytek M. 2006. Environmental Controls on Denitrifying Communities and Denitrification Rates: Insights from Molecular Methods. Ecological Applications 16:2143–2152.

36. Herbert ER, Schubauer-Berigan J, Craft CB. 2018. Differential effects of chronic and acute simulated seawater intrusion on tidal freshwater marsh carbon cycling. Biogeochemistry 138:137–154.

37. Colmer TD. 2003. Long-distance transport of gases in plants: a perspective on internal aeration and radial oxygen loss from roots. Plant, Cell & Environment 26:17–36.

38. Cook FJ, Knight JH. 2003. Oxygen Transport to Plant Roots. Soil Science Society of America Journal 67:20–31.

39. Koop-Jakobsen K, Wenzhöfer F. 2015. The Dynamics of Plant-Mediated Sediment Oxygenation in Spartina anglica Rhizospheres—a Planar Optode Study. Estuaries and Coasts 38:951–963.

40. Burgin AJ, Hamilton SK. 2008. NO3−-Driven SO42− Production in Freshwater Ecosystems: Implications for N and S Cycling. Ecosystems 11:908–922.

41. Lamers LPM, Govers LL, Janssen ICJM, Geurts JJM, Van der Welle MEW, Van Katwijk MM, Van der Heide T, Roelofs JGM, Smolders AJP. 2013. Sulfide as a soil phytotoxin—a review. Front Plant Sci 4:268.

42. Weber KA, Achenbach LA, Coates JD. 2006. Microorganisms pumping iron: anaerobic microbial iron oxidation and reduction. 10. Nat Rev Microbiol 4:752–764.

43. Ardón M, Morse JL, Doyle MW, Bernhardt ES. 2010. The Water Quality Consequences of Restoring Wetland Hydrology to a Large Agricultural Watershed in the Southeastern Coastal Plain. Ecosystems 13:1060–1078.

44. Morse JL, Ardón M, Bernhardt ES. 2012. Greenhouse gas fluxes in southeastern U.S. coastal plain wetlands under contrasting land uses. Ecological Applications 22:264–280.

45. Hoffmann M, Pehle N, Huth V, Jurisch N, Sommer M, Augustin J. 2018. A simple method to assess the impact of sealing, headspace mixing and pressure vent on airtightness of manually closed chambers. Journal of Plant Nutrition and Soil Science 181:36–40.

46. R Core Team. 2024. R: A Language and Environment for Statistical Computing (4.4.2 (2024-10-31) -- “Pile of Leaves”). R Foundation for Statistical Computing, Vienna, Austria.

47. Fuss R, Hueppi R. 2024. gasfluxes: Greenhouse Gas Flux Calculation from Chamber Measurements (0.6-2).

48. Peralta AL, Bledsoe RB, Muscarella ME, Huntemann M, Clum A, Foster B, Foster B, Roux S, Palaniappan K, Varghese N, Mukherjee S, Reddy TBK, Daum C, Copeland A, Chen I-MA, Ivanova NN, Kyrpides NC, Glavina del Rio T, Eloe-Fadrosh EA. 2020. Metagenomes from Experimental Hydrologic Manipulation of Restored Coastal Plain Wetland Soils (Tyrell County, North Carolina). Microbiol Resour Announc 9.

49. Bledsoe RB, Finlay CG, Peralta AL. 2024. Plant-microbe-mediated decrease of greenhouse gases under dynamic wetland hydrology. bioRxiv https://doi.org/10.1101/2020.06.29.178533.

50. Bowers RM, Kyrpides NC, Stepanauskas R, Harmon-Smith M, Doud D, Reddy TBK, Schulz F, Jarett J, Rivers AR, Eloe-Fadrosh EA, Tringe SG, Ivanova NN, Copeland A, Clum A, Becraft ED, Malmstrom

RR, Birren B, Podar M, Bork P, Weinstock GM, Garrity GM, Dodsworth JA, Yooseph S, Sutton G, Glöckner FO, Gilbert JA, Nelson WC, Hallam SJ, Jungbluth SP, Ettema TJG, Tighe S, Konstantinidis KT, Liu W-T, Baker BJ, Rattei T, Eisen JA, Hedlund B, McMahon KD, Fierer N, Knight R, Finn R, Cochrane G, Karsch-Mizrachi I, Tyson GW, Rinke C, Lapidus A, Meyer F, Yilmaz P, Parks DH, Murat Eren A, Schriml L, Banfield JF, Hugenholtz P, Woyke T. 2017. Minimum information about a single amplified genome (MISAG) and a metagenome-assembled genome (MIMAG) of bacteria and archaea. 8. Nat Biotechnol 35:725–731.

51. Chen I-MA, Markowitz VM, Chu K, Palaniappan K, Szeto E, Pillay M, Ratner A, Huang J, Andersen E, Huntemann M, Varghese N, Hadjithomas M, Tennessen K, Nielsen T, Ivanova NN, Kyrpides NC. 2017. IMG/M: integrated genome and metagenome comparative data analysis system. Nucleic Acids Research 45:D507–D516.

52. Garber AI, Nealson KH, Okamoto A, McAllister SM, Chan CS, Barco RA, Merino N. 2020. FeGenie: A Comprehensive Tool for the Identification of Iron Genes and Iron Gene Neighborhoods in Genome and Metagenome Assemblies. Frontiers in Microbiology 11.

53. Jenkinson BJ, Franzmeier DP. 2006. Development and Evaluation of Iron-Coated Tubes that Indicate Reduction in Soils. Soil Science Society of America Journal 70:183–191.

54. Schneider CA, Rasband WS, Eliceiri KW. 2012. NIH Image to ImageJ: 25 years of image analysis. Nature Methods 9:671–675.

55. Mehlich A. 1984. Mehlich 3 soil test extractant: A modification of Mehlich 2 extractant. Communications in Soil Science and Plant Analysis 15:1409–1416.

56. Schneider G, Chicken E, Becvarik R. 2024. NSM3: Functions and Datasets to Accompany Hollander, Wolfe, and Chicken - Nonparametric Statistical Methods, Third Edition (1.19).

57. Oksanen J, Simpson G, Blanchet F, Kindt R, Legendre P, Minchin P, O'Hara R, Solymos P, Stevens M, Szoecs E, Wagner H, Barbour M, Bedward M, Bolker B, Borcard D, Carvalho G, Chirico M, De Caceres M, Durand S, Evangelista H, FitzJohn R, Friendly M, Furneaux B, Hannigan G, Hill M, Lahti L, McGlinn D, Ouellette M, Ribeiro Cunha, Smith T, Stier A, Ter Braak C, Weedon J. 2022. vegan: Community Ecology Package (R package version 2.6-4). R.

58. Klassen J, Allen DM. 2017. Assessing the risk of saltwater intrusion in coastal aquifers. Journal of Hydrology 551:730–745.

59. Ghosh W, Dam B. 2009. Biochemistry and molecular biology of lithotrophic sulfur oxidation by taxonomically and ecologically diverse bacteria and archaea. FEMS Microbiology Reviews 33:999–1043.

60. Rückert C. 2016. Sulfate reduction in microorganisms—recent advances and biotechnological applications. Current Opinion in Microbiology 33:140–146.

61. Smyth AR, Thompson SP, Siporin KN, Gardner WS, McCarthy MJ, Piehler MF. 2013. Assessing Nitrogen Dynamics Throughout the Estuarine Landscape. Estuaries and Coasts 36:44–55.

62. Jia M, Winkler MKH, Volcke EIP. 2020. Elucidating the Competition between Heterotrophic Denitrification and DNRA Using the Resource-Ratio Theory. Environ Sci Technol 54:13953–13962.

63. Koop-Jakobsen K, Giblin AE. 2010. The effect of increased nitrate loading on nitrate reduction via denitrification and DNRA in salt marsh sediments. Limnology and Oceanography 55:789–802.

64. Li S, Jiang Z, Ji G. 2022. Effect of sulfur sources on the competition between denitrification and DNRA. Environmental Pollution 305:119322.

65. Canfield DE, Jørgensen BB, Fossing H, Glud R, Gundersen J, Ramsing NB, Thamdrup B, Hansen JW, Nielsen LP, Hall POJ. 1993. Pathways of organic carbon oxidation in three continental margin sediments. Marine Geology 113:27–40.

66. Flynn TM, Antonopoulos DA, Skinner KA, Brulc JM, Johnston E, Boyanov MI, Kwon MJ, Kemner KM, O'Loughlin EJ. 2021. Biogeochemical dynamics and microbial community development under sulfate- and iron-reducing conditions based on electron shuttle amendment. PLOS ONE 16:e0251883.

67. Sivan O, Shusta SS, Valentine DL. 2016. Methanogens rapidly transition from methane production to iron reduction. Geobiology 14:190–203.

68. van Bodegom PM, Scholten JCM, Stams AJM. 2004. Direct inhibition of methanogenesis by ferric iron. FEMS Microbiology Ecology 49:261–268.

69. Lyu Z, Shao N, Akinyemi T, Whitman WB. 2018. Methanogenesis. Current Biology 28:R727–R732.

70. Sivan O, Shusta SS, Valentine DL. 2016. Methanogens rapidly transition from methane production to iron reduction. Geobiology 14:190–203.

71. Conrad R. 1999. Contribution of hydrogen to methane production and control of hydrogen concentrations in methanogenic soils and sediments. FEMS Microbiology Ecology 28:193–202.

72. Schink B. 1997. Energetics of syntrophic cooperation in methanogenic degradation. Microbiology and Molecular Biology Reviews 61:262–280.

73. Chidthaisong A, Conrad R. 2000. Turnover of glucose and acetate coupled to reduction of nitrate, ferric iron and sulfate and to methanogenesis in anoxic rice field soil. FEMS Microbiology Ecology 31:73–86.

74. Kiene RP, Oremland RS, Catena A, Miller LG, Capone DG. 1986. Metabolism of Reduced Methylated Sulfur Compounds in Anaerobic Sediments and by a Pure Culture of an Estuarine Methanogen. Applied and Environmental Microbiology 52:1037–1045.

75. Oremland RS, Polcin S. 1982. Methanogenesis and Sulfate Reduction: Competitive and Noncompetitive Substrates in Estuarine Sediments. Applied and Environmental Microbiology 44:1270–1276.

76. Bueno de Mesquita CP, Hartman WH, Ardón M, Tringe SG. 2024. Disentangling the effects of sulfate and other seawater ions on microbial communities and greenhouse gas emissions in a coastal forested wetland. ISME Communications 4:ycae040.

77. Bryant MP, Campbell LL, Reddy CA, Crabill MR. 1977. Growth of Desulfovibrio in Lactate or Ethanol Media Low in Sulfate in Association with H2-Utilizing Methanogenic Bacteria. Applied and Environmental Microbiology 33:1162–1169.

78. Koster IW, Rinzema A, de Vegt AL, Lettinga G. 1986. Sulfide inhibition of the methanogenic activity of granular sludge at various pH-levels. Water Research 20:1561–1567.

79. Mountfort DO, Asher RA. 1979. Effect of inorganic sulfide on the growth and metabolism of Methanosarcina barkeri strain DM. Applied and Environmental Microbiology 37:670–675.

80. Shi X, Gao G, Tian J, Wang XC, Jin X, Jin P. 2020. Symbiosis of sulfate-reducing bacteria and methanogenic archaea in sewer systems. Environment International 143:105923.

81. Bethke CM, Sanford RA, Kirk MF, Jin Q, Flynn TM. 2011. The thermodynamic ladder in geomicrobiology. American Journal of Science 311:183–210.

FIGURES AND TABLES

Figure 1

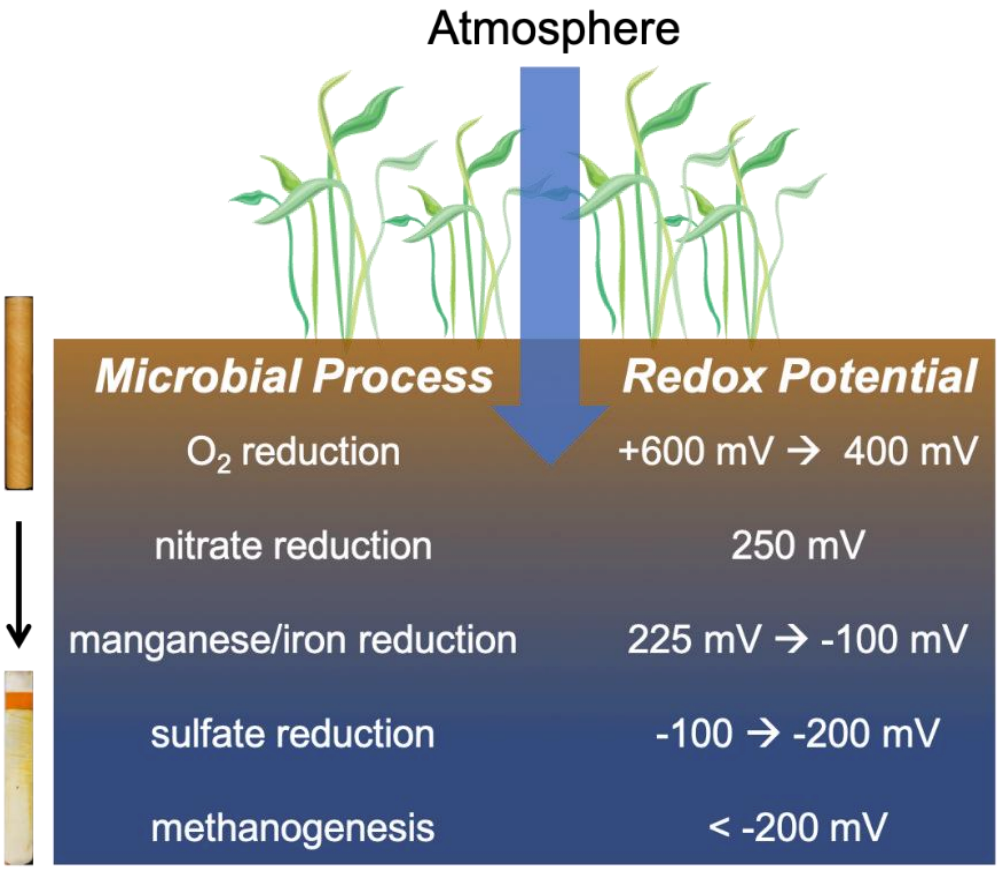

Figure 1. Conceptual diagram depicting relative ranges of redox potentials associated with predicted microbial processes. On the left side of the diagram, indicator for reduction in soils (IRIS) tubes are used to measure soil redox status, where iron oxide paint in orange represents oxidized (Fe(III)) conditions, and white represents reduced (Fe(II)) conditions.

Figure 2

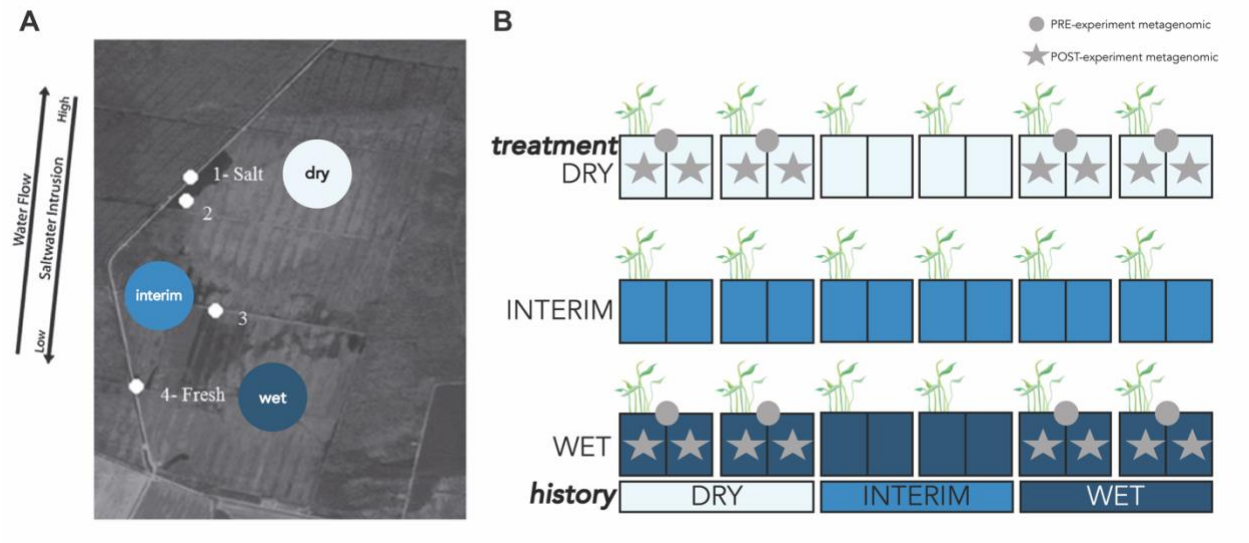

Figure 2. Field site sampling and experimental design of wetland mesocosm experiment. Wetland mesocosms sourced from the Timberlake Observatory for Wetland Restoration field site (image modified from Schoepfer et al., 2014), with hydrologic histories for present study (dry, interim, wet) labeled with circles (A). Numbered white dots on the map indicate the sampling locations from Schoepfer et al, 2014, and the determination of salt and freshwater conditions during sampling in 2012 (15). The schematic on the right shows each replicate of the mesocosm experiment, with grey circles representing mesocosms sampled for pre-experiment metagenomics (n = 8), and grey stars representing mesocosms sampled for post-experiment metagenomics (n = 16).

Figure 3

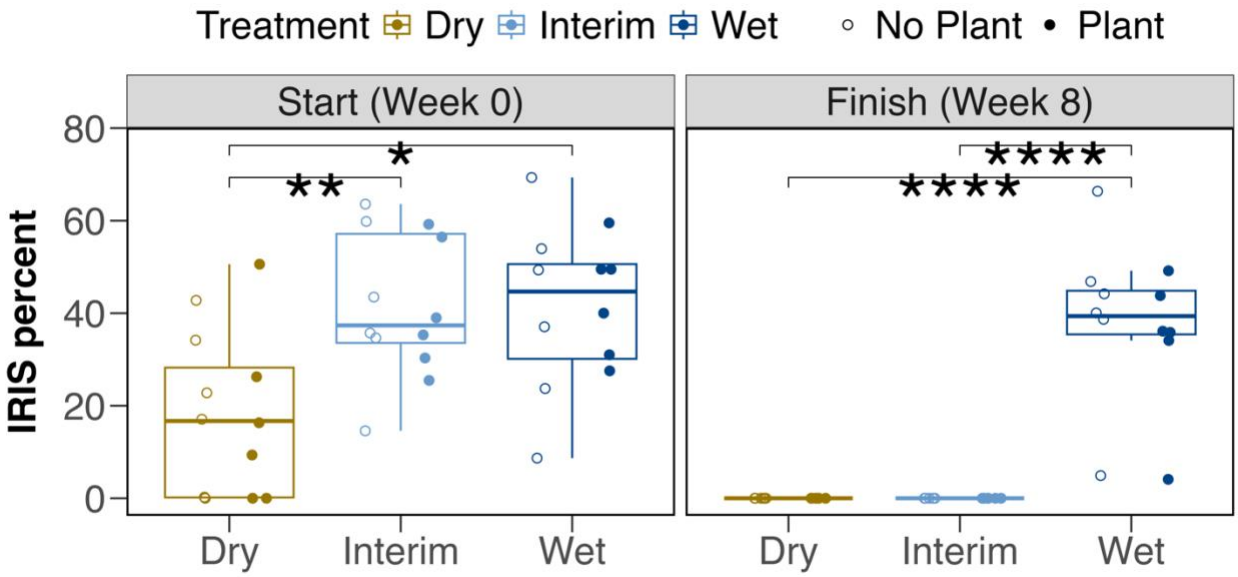

Figure 3. Percent paint removed from IRIS tubes at start (week 0) and finish (week 8) of experimental incubation. More reducing conditions correspond to a higher percent of paint removed from IRIS tubes ("IRIS percent"). Individual data points from IRIS tubes are plotted as points; symbol color represents hydrologic treatment, open points = no plant, and closed points = plant. The boxplot is a visual representation the following summary statistics: the median, the 25th and 75th percentiles, and the whiskers which represent 1.5 × the interquartile range. Asterisks and brackets represent significance levels of pairwise comparisons using the Dwass-Steel-Critchlow-Fligner procedure: ****: $p \leq 0.0001$, **: $p \leq 0.01$, *: $p \leq 0.05$, no asterisk: nonsignificant. Figure modified from Bledsoe et al., 2023 (49).

Figure 4

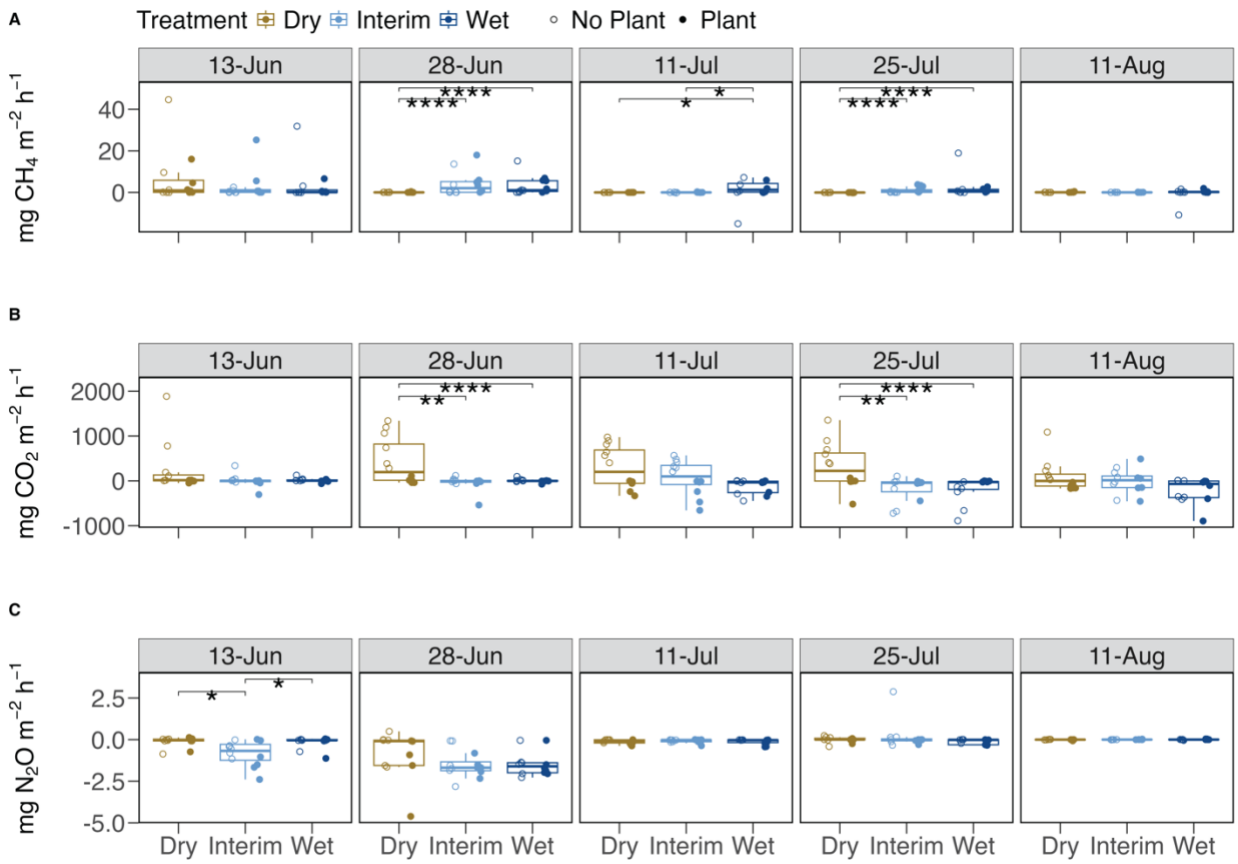

Figure 4. Greenhouse gas fluxes measured under different hydrologic conditions over time. Fluxes are in milligram of greenhouse gas per square meter per hour. Color represents hydrologic treatment (brown = dry, light blue = interim, dark blue = wet). Individual fluxes are plotted, and fill represents plant presence/absence: open point = no plant, filled point = plant. Boxplots summarize median, first and third quartiles, and two whiskers extending |≤| 1.5 * interquartile range. Asterisks and brackets represent significance levels of pairwise comparisons using the Dwass-Steel-Critchlow-Fligner procedure: ****: $p \leq 0.0001$, **: $p \leq 0.01$, *: $p \leq 0.05$, no asterisk: nonsignificant. An extreme outlier of 248 mg CH_4 m^{-2} h^{-1}, measured in a wet treatment with no

plants on July 11th was used in statistical calculations but not displayed in the plot to improve visualization of differences across treatments.

Figure 5

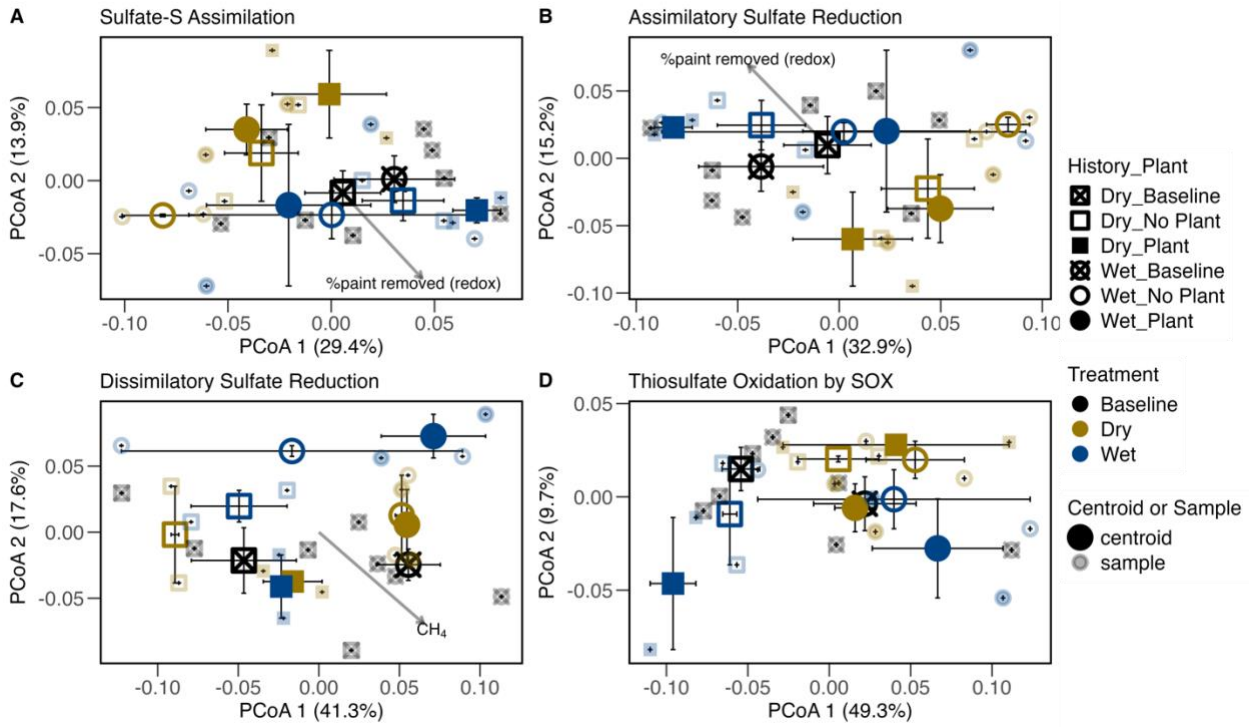

Figure 5. Ordination of sulfur functional gene modules. Ordinations are based on principal coordinates analysis (PCoA), depicting community composition of the sulfur functional gene modules Sulfate-Sulfur Assimilation (M00616) (A), Assimilatory Sulfate Reduction (M00176) (B), Dissimilatory Sulfate Reduction (M00596) (C), and Thiosulfate Oxidation by SOX Complex (M00595) (D). Percent variance explained by each axis is listed in parentheses. Colors refer to hydrologic treatments, where black = baseline, brown = dry, dark blue = wet. Shapes refer to hydrologic history of the sample, where square = dry, circle = wet. The shape fill represents plant treatment, where 'x' through symbol = baseline, open symbol = no plant, closed symbol = plant. Baseline samples were collected before the start of hydrologic and plant treatments and treatment samples were collected after eight weeks. Vectors represent significant ($p \leq 0.05$) correlation between greenhouse gas trends or soil redox status (as measured by percent paint removed from IRIS tubes) and functional gene composition, scaled by magnitude of correlation (using envfit).

Figure 6

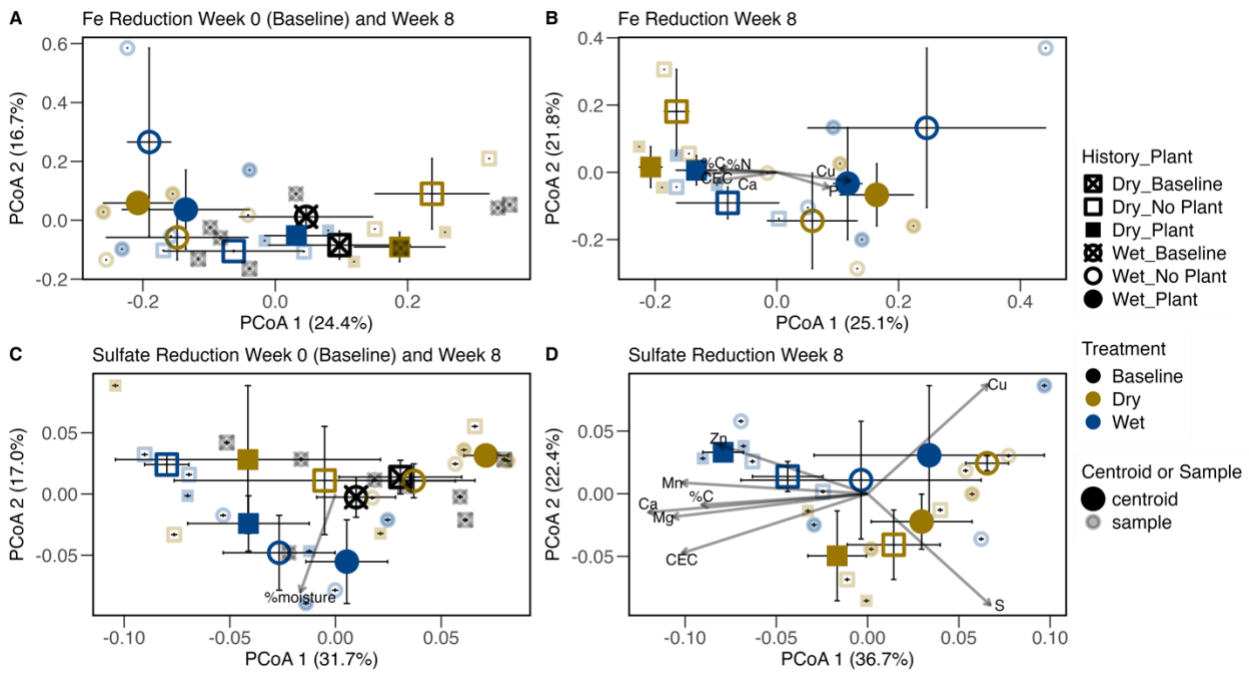

Figure 6. Ordination of iron reduction and sulfur reduction genes. Ordinations are based on principal coordinates analysis (PCoA), depicting community composition of the functional gene modules: Fe reduction genes identified by FeGenie at Week 0 and Week 8 of the 8-week experiment (A), Fe reduction genes identified by FeGenie at end of 8-week experiment (B), sulfate reduction genes (both assimilatory and dissimilatory) at Week 0 and Week 8 of 8-week experiment (C), and sulfate reduction genes (both assimilatory and dissimilatory) at end of 8-week experiment (D). Percent variance explained by each axis is listed in parentheses. Colors refer to hydrologic treatments, where black = baseline, brown = dry, dark blue = wet. Shapes refer to hydrologic history of the sample, where square = dry, circle = wet. The shape fill represents plant treatment, where 'x' through symbol = baseline, open symbol = no plant, closed symbol = plant. Baseline samples were collected before the start of hydrologic and plant treatments and treatment samples were collected after eight weeks. Vectors represent significant ($p \leq 0.05$) correlation between

greenhouse gas trends or soil physicochemical parameters, and functional gene composition, scaled by magnitude of correlation (using envfit).

Figure 7

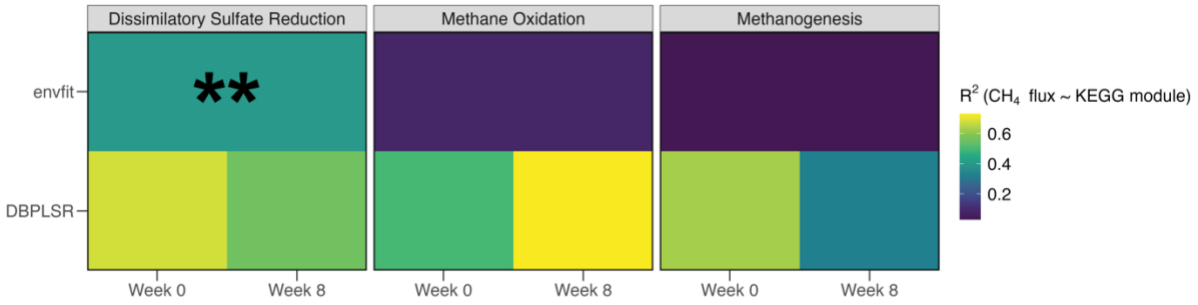

Figure 7. Methane flux as a function of functional gene composition. The KEGG modules analyzed were M00596 (Dissimilatory Sulfate Reduction), M00174 (Methane Oxidation), and M00617 (Methanogen). Envfit was used to assess relationships between methane flux and the principal coordinate analysis (PCoA) of respective Kyoto Encyclopedia of Genes and Genomes (KEGG) modules and include pre- ("Week 0") and post-experiment ("Week 8") samples. Asterisks on envfit represent significance thresholds: ** = $p \leq 0.01$, no label = $p > 0.05$. In the distance-based partial least squares regression (DBPLSR), week 0 and week 8 relationships were analyzed separately. There are no p-values or significance levels for DBPLSR. Color represents the R^2 for either envfit or DBPLSR (adjusted R^2, two component model for DBPLSR).

Figure 8

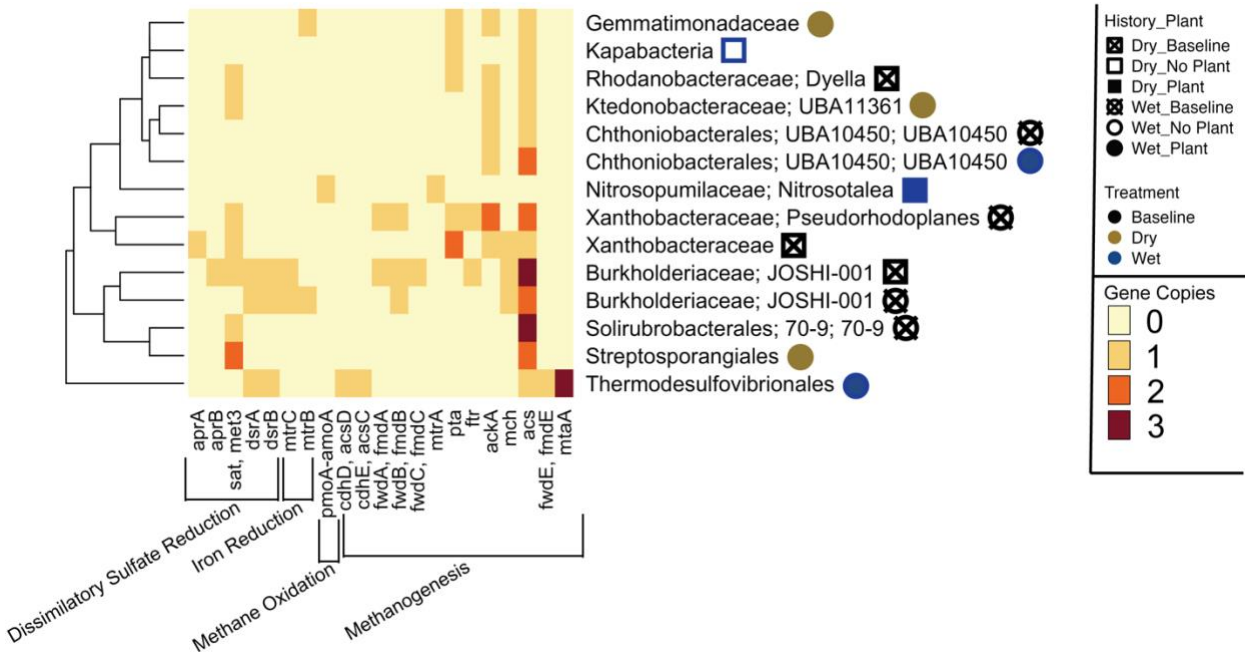

Figure 8. Heatmap of functional genes found in metagenome bins. Symbols next to bin taxonomy show the environment the bin was sourced from: colors refer to hydrologic treatments (brown = dry, dark blue = wet), shapes refer to hydrologic history (square = dry, circle = wet), and the shape fill represents plant treatment (open symbol = no plant, closed symbol = plant). Heatmap colors indicate the number of gene copies found in a metagenome bin. The dendrogram on the left side is calculated based on the similarity of the gene counts in the functional modules listed on the bottom of the heatmap. The functional gene modules are based on KEGG Dissimilatory Sulfate Reduction (M00596), TIGRFAMS mtrBC (TIGR03509, TIGR03507), KEGG Methane Oxidation (M00174), and KEGG Methanogen (M00617). The complete set of genes in each module was queried, but only genes with at least one hit in one bin are included in the heatmap.

Table 1. Summary of differences in community functional gene composition. Permutational multivariate analysis of variance (PERMANOVA) was used to compare treatment differences in key functional categories, and differences in composition ($p \leq 0.05$) are marked with an asterisk. Kyoto Encyclopedia of Genes and Genomes (KEGG) numbers are listed in parentheses for KEGG Modules. Iron genes were annotated using FeGenie and TIGRFAMS.

Gene Module	Plant	History	Treatment
Sulfate-Sulfur Assimilation (KEGG M00616)			*
Assimilatory Sulfate Reduction (KEGG M00176)			*
Dissimilatory Sulfate Reduction (KEGG M00596)		*	
Sulfate Reduction (combined assimilatory and dissimilatory)		*	*
Thiosulfate Oxidation by SOX Complex (KEGG M00595)		*	
Fe Genes (FeGenie)		*	
Fe Reduction (FeGenie)		*	
Fe Reduction (TIGRFAMS mtrBC)	*		*
Dissimilatory Nitrate Reduction to Ammonium (DNRA) (KEGG M00530)			
Methane Oxidation (KEGG M00174)			

Appendix S1

Hydrologic history and short-term flooding control iron and sulfur metabolic composition with variable associations to greenhouse gas production in a coastal wetland mesocosm experiment

Colin G. Finlay[a]#, Ariane L. Peralta,[a]

[a] Department of Biology, East Carolina University, Greenville, North Carolina, USA

Running Head: Microbial response to hydrology and flooding pulses

#Address correspondence to Colin G. Finlay, finlayc21@students.ecu.edu.

TABLES

Table A1. Summary of PERMANOVA comparing microbial community composition due to main effects (plant, hydrologic history, hydrologic treatment) and interaction between plant × history and plant × treatment.

Gene Module	Main Effect	DF	SumSq	R^2	F	p
Sulfate-Sulfur Assimilation (KEGG M00616)	Plant	2	0.006	0.066	0.891	0.527
	History	1	0.005	0.061	1.654	0.153
	Treatment	1	**0.013**	**0.144**	**3.917**	**0.008**
	Plant × History	2	0.008	0.090	1.228	0.276
	Plant × Treatment	1	0.004	0.051	1.389	0.222
Assimilatory Sulfate Reduction (KEGG M00176)	Plant	2	0.006	0.066	0.872	0.514
	History	1	0.004	0.046	1.221	0.288
	Treatment	1	**0.015**	**0.156**	**4.111**	**0.013**
	Plant × History	2	0.009	0.091	1.193	0.307
	Plant × Treatment	1	0.003	0.031	0.817	0.497
Dissimilatory Sulfate Reduction (KEGG M00596)	Plant	2	0.012	0.113	1.859	0.132
	History	1	**0.032**	**0.316**	**10.397**	**3e-4**
	Treatment	1	0.003	0.029	0.947	0.388
	Plant × History	2	0.005	0.046	0.755	0.577
	Plant × Treatment	1	0.001	0.010	0.3171	0.784
Sulfate Reduction (combined assimilatory and dissimilatory)	Plant	2	0.007	0.060	0.786	0.619
	History	1	**0.012**	**0.108**	**2.830**	**0.033**
	Treatment	1	**0.013**	**0.111**	**2.906**	**0.026**
	Plant × History	2	0.009	0.077	1.016	0.418
	Plant × Treatment	1	0.004	0.034	0.879	0.476
Thiosulfate Oxidation by SOX Complex (KEGG M00595)	Plant	2	0.004	0.045	0.608	0.637
	History	1	**0.022**	**0.243**	**6.547**	**0.009**
	Treatment	1	0.007	0.078	2.095	0.135
	Plant × History	2	0.002	0.017	0.234	0.939
	Plant × Treatment	1	0.002	0.024	0.656	0.501
Fe Genes (FeGenie)	Plant	2	0.001	0.028	0.315	0.880
	History	1	**0.006**	**0.185**	**4.173**	**0.031**
	Treatment	1	0.001	0.044	0.994	0.354
	Plant × History	2	0.001	0.028	0.318	0.872
	Plant × Treatment	1	2.01e-4	0.006	0.139	0.909
Fe Reduction (FeGenie)	Plant	2	0.157	0.094	1.189	0.280
	History	1	**0.221**	**0.132**	**3.358**	**0.004**
	Treatment	1	0.010	0.060	1.513	0.161

	Plant × History	2	0.102	0.061	0.772	0.700
	Plant × Treatment	1	0.038	0.023	0.580	0.787
Fe Reduction (TIGRFAMS mtrBC)	**Plant**	2	**0.032**	**0.335**	**9.967**	**0.002**
	History	1	0.004	0.037	2.187	0.162
	Treatment	1	**0.031**	**0.319**	**19.012**	**6.9e-4**
	Plant × History	2	0.003	0.036	1.058	0.367
	Plant × Treatment	1	4.66e-4	0.005	0.288	0.598
Dissimilatory Nitrate Reduction to Ammonium (DNRA) (KEGG M00530)	Plant	2	0.014	0.115	1.282	0.270
	History	1	0.004	0.035	0.773	0.529
	Treatment	1	0.006	0.049	1.090	0.355
	Plant × History	2	0.009	0.079	0.881	0.518
	Plant × Treatment	1	0.001	0.007	0.156	0.951
Methane Oxidation (KEGG M00174)	Plant	2	0.171	0.085	0.878	0.542
	History	1	0.051	0.025	0.518	0.704
	Treatment	1	0.023	0.012	0.240	0.888
	Plant × History	2	0.129	0.064	0.663	0.701
	Plant × Treatment	1	0.083	0.041	0.851	0.490

Notes: Bold text indicates significant differences ($p \leq 0.05$).

Abbreviations: PERMANOVA: permutational multivariate analysis of variance, DF: degrees of freedom, KEGG: Kyoto Encyclopedia of Genes and Genomes, SumSq: sum of squares.

Table A2. Summary of distance-based partial least squares regression representing percent of variance in greenhouse gas fluxes explained by the first two components of models derived from functional gene composition.

GHG ~ Gene module	Timepoint	n components total	Statistic	Comp 1	Comp 2
CH_4 ~ Dissimilatory Sulfate Reduction	Start	7	R^2	0.60	0.77
			adjusted R^2	0.53	0.68
			gvar	67.13	86.25
			crit	5.12	3.93
CH_4 ~ Dissimilatory Sulfate Reduction	Finish	15	R^2	0.46	0.62
			adjusted R^2	0.42	0.56
			gvar	53.15	85.41
			crit	0.28	0.23
CH_4 ~ Methane Oxidation	Start	7	R^2	0.44	0.64
			adjusted R^2	0.35	0.50
			gvar	76.22	86.27
			crit	7.16	6.28
CH_4 ~ Methane Oxidation	Finish	15	R^2	0.63	0.77
			adjusted R^2	0.61	0.73
			gvar	29.28	84.80
			crit	0.19	0.14
CH_4 ~ Methanogenesis	Start	7	R^2	0.52	0.74
			adjusted R^2	0.44	0.63
			gvar	26.04	62.04
			crit	6.10	4.56
CH_4 ~ Methanogenesis	Finish	15	R^2	0.19	0.42
			adjusted R^2	0.13	0.33
			gvar	35.78	58.00
			crit	0.43	0.35

Notes: The total number of components in each model (n components total) is equal to sample size minus one, similar to degrees of freedom. Functional gene distance matrices are based on the Bray-Curtis dissimilarities of gene relative abundances within respective KEGG modules (see main text for KEGG module numbers).

Abbreviations: GHG: greenhouse gas, comp: component, gvar: total weighted geometric variability, crit: generalized cross validation critical value.

Table A3. Mantel test for correlation among paired Bray-Curtis distance matrices of functional gene modules. The Mantel correlation (r) is based on Pearson's product-moment correlation. Bold text indicates significant correlations ($p \leq 0.05$).

X Distance Matrix	Y Distance Matrix	Mantel correlation *r*	*p*
Fe Reduction (FeGenie)	SO_4^{2-} Reduction (Assimilatory and Dissimilatory)	0.064	0.249
Fe Reduction (FeGenie)	**Assimilatory SO_4^{2-} Reduction**	**0.222**	**0.008**
Fe Reduction (FeGenie)	**Dissimilatory SO_4^{2-} Reduction**	**0.313**	**0.006**
Denitrification	Thiosulfate Oxidation by SOX Complex	0.117	0.170
DNRA	**Thiosulfate Oxidation by SOX Complex**	**0.196**	**4.990e-2**

Abbreviations. SOX: thiosulfate oxidizing multienzyme complex, DNRA: dissimilatory nitrate reduction to ammonium.

Table A4. Hydrology-specific Mantel test for correlation among paired Bray-Curtis distance matrices of functional gene modules. The Mantel correlation (r) is based on Pearson's product-moment correlation. Distance matrices were subset according to wet history, dry history, wet treatment, and dry treatment. Mantel tests were then performed on sulfate reduction and iron reduction distance matrices in each respective hydrologic condition, e.g., wet history. Bold text indicates significant correlations ($p \leq 0.05$).

X Distance Matrix	Y Distance Matrix	Wet History	Dry History	Wet Treatment	Dry Treatment
Sulfate Reduction	Iron Reduction	r = 0.148, p = 0.214	r = 0.010, p = 0.446	**r = 0.360, p = 0.010**	r = -0.166, p = 0.728

Table A5. Summary of metagenome bins. Binning was performed using the IMG pipeline (MetaBAT, CheckM, GTDB, GTDB-tk). Bins are accessible at https://img.jgi.doe.gov/, under the Bin ID.

Bin ID	History	Treatment	Plant Presence/ Absence	Bin Quality	GTDBTK Lineage	Bin Completeness	Bin Contamination	Total Bases	Gene Count
3300036865_5	Dry	Baseline	Baseline	MQ	Bacteria; Proteobacteria; Gammaproteobacteria; Betaproteobacteriales; Burkholderiaceae; JOSHI-001	88.02	6.17	4674782	4849
3300036991_3	Dry	Baseline	Baseline	HQ	Bacteria; Proteobacteria; Gammaproteobacteria; Xanthomonadales; Rhodanobacteraceae; Dyella	98.45	2.71	4930595	4528
3300036991_4	Dry	Baseline	Baseline	MQ	Bacteria; Proteobacteria; Alphaproteobacteria; Rhizobiales; Xanthobacteraceae	54.51	1.92	2325436	2615
3300036870_7	Dry	Wet	Plant	MQ	Archaea; Crenarchaeota; Nitrososphaeria; Nitrososphaerales; Nitrosopumilaceae; Nitrosotalea	61	0.97	780222	1032
3300036873_3	Dry	Wet	No Plant	HQ	Bacteria; Bacteroidota; Kapabacteria	96.98	1.64	3157872	2807
3300036867_3	Wet	Baseline	Baseline	MQ	Bacteria; Proteobacteria; Gammaproteobacteria; Betaproteobacteriales; Burkholderiaceae; JOSHI-001	76.88	0.7	3880859	4065

3300036989_2	Wet	Baseline	Baseline	MQ	Bacteria; Proteobacteria; Alphaproteobacteria; Rhizobiales; Xanthobacteraceae; Pseudorhodoplanes	62.92	8.67	3626868	4149
3300036989_4	Wet	Baseline	Baseline	MQ	Bacteria; Actinobacteriota; Thermoleophilia; Solirubrobacterales; 70-9; 70-9	80.23	5.11	2422891	2808
3300036990_3	Wet	Baseline	Baseline	MQ	Bacteria; Verrucomicrobiota; Verrucomicrobiae; Chthoniobacterales; UBA10450; UBA10450	61.4	0.72	2180017	2388
3300036875_5	Wet	Dry	Plant	MQ	Bacteria; Actinobacteriota; Actinobacteria; Streptosporangiales	51.1	8.78	3331403	3616
3300036898_4	Wet	Dry	Plant	MQ	Bacteria; Chloroflexota; Ktedonobacteria; Ktedonobacterales; Ktedonobacteraceae; UBA11361	85.26	1.98	4109904	4252
3300036898_5	Wet	Dry	Plant	MQ	Bacteria; Gemmatimonadota; Gemmatimonadetes; Gemmatimonadales; Gemmatimonadaceae	64.48	6.41	3359397	3472
3300036872_8	Wet	Wet	Plant	MQ	Bacteria; Nitrospirota; Thermodesulfovibrionia; Thermodesulfovibrionales	56.04	0.36	1448797	1708
3300036993_3	Wet	Wet	No Plant	MQ	Bacteria; Verrucomicrobiota; Verrucomicrobiae; Chthoniobacterales; UBA10450; UBA10450	74.22	4.2	3077671	3555

Abbreviations: MQ = medium quality, HQ = high quality